ORIGINAL ARTICLE

Desmosomal Hyper-Adhesion Affects Direct Inhibition of Desmoglein Interactions in Pemphigus

JID Open

Letyfee Steinert[1], Michael Fuchs[1], Anna M. Sigmund[1], Dario Didona[2], Christoph Hudemann[2], Christian Möbs[2], Michael Hertl[2], Takashi Hashimoto[3], Jens Waschke[1] and Franziska Vielmuth[1]

During differentiation, keratinocytes acquire a strong, hyper-adhesive state, where desmosomal cadherins interact calcium ion independently. Previous data indicate that hyper-adhesion protects keratinocytes from pemphigus vulgaris autoantibody–induced loss of intercellular adhesion, although the underlying mechanism remains to be elucidated. Thus, in this study, we investigated the effect of hyper-adhesion on pemphigus vulgaris autoantibody–induced direct inhibition of desmoglein (DSG) 3 interactions by atomic force microscopy. Hyper-adhesion abolished loss of intercellular adhesion and corresponding morphological changes of all pathogenic antibodies used. Pemphigus autoantibodies putatively targeting several parts of the DSG3 extracellular domain and 2G4, targeting a membrane-proximal domain of DSG3, induced direct inhibition of DSG3 interactions only in non-hyper-adhesive keratinocytes. In contrast, AK23, targeting the N-terminal extracellular domain 1 of DSG3, caused direct inhibition under both adhesive states. However, antibody binding to desmosomal cadherins was not different between the distinct pathogenic antibodies used and was not changed during acquisition of hyper-adhesion. In addition, heterophilic DSC3–DSG3 and DSG2–DSG3 interactions did not cause reduced susceptibility to direct inhibition under hyper-adhesive condition in wild-type keratinocytes. Taken together, the data suggest that hyper-adhesion reduces susceptibility to autoantibody-induced direct inhibition in dependency on autoantibody-targeted extracellular domain but also demonstrate that further mechanisms are required for the protective effect of desmosomal hyper-adhesion in pemphigus vulgaris.

Keywords: Desmoglein 3, Desmosome, Hyper-adhesion, Keratinocyte, Pemphigus vulgaris

Journal of Investigative Dermatology (2024) **144,** 2682–2694; doi:10.1016/j.jid.2024.03.042

INTRODUCTION

Desmosomes are highly specialized adhesion complexes required to withstand mechanical stress in tissues constantly facing mechanical load such as the epidermis, the intestine, and the myocardium (Berika and Garrod, 2014; Price et al, 2018). On a molecular level, desmosomal adhesion is based on homophilic and heterophilic interactions of desmosomal cadherins, desmogleins (DSGs) 1–4 and desmocollins (DSCs) 1–3, which reveal a tissue- and differentiation-specific expression pattern (Hegazy et al, 2022). The adhesive function of desmosomal cadherins is maintained by their extracellular domain (ECD), which consists of 4 ECDs and an extracellular anchor (Garrod and Chidgey, 2008; Owen and Stokes, 2010). Intracellularly, desmosomal plaque proteins link desmosomal cadherins to the keratin cytoskeleton (Cheng and Koch, 2004; Getsios et al, 2004; Green and Simpson, 2007).

The importance of desmosomes is reflected in pemphigus vulgaris (PV), a bullous autoimmune dermatosis in which pathogenic autoantibodies against the desmosomal cadherins, DSG1 and DSG3 as well as DSC3, cause blisters of the skin and mucous membranes (Kasperkiewicz et al, 2017; Schmidt et al, 2019; Waschke and Spindler, 2014). The mechanisms through which PV-IgGs induce loss of intercellular adhesion in keratinocytes (KCs) comprise direct inhibition of DSG3 interactions as well as dysregulation of a plethora of signaling pathways (Spindler et al, 2018; Spindler and Waschke, 2018). Direct inhibition summarizes mechanisms that disrupt DSG interaction either caused by steric hindrance or allosteric effects (Vielmuth et al, 2018b; Waschke et al, 2005). Changes in desmosomal cadherin single-molecule–binding properties contribute to loss of intercellular adhesion in pemphigus (Vielmuth et al, 2018a). Pemphigus autoantibodies directly inhibit DSG3 but not DSG1 interactions (Heupel et al, 2008; Vielmuth et al, 2018b, 2015; Waschke et al, 2005) and cause a redistribution of DSG1 away from sides of cell–cell contact (Vielmuth et al, 2018b).

During maturation, desmosomes adopt a strong adhesive state, referred to as hyper-adhesive in which desmosomal cadherins acquire calcium ion (Ca^{2+}) independency. DSG3 is

[1]Vegetative Anatomy, Institute of Anatomy, Faculty of Medicine, Ludwig Maximilian University of Munich, Munich, Germany; [2]Department of Dermatology and Allergology, Philipps-Universität Marburg, Marburg, Germany; and [3]Department of Dermatology, Graduate School of Medicine, Osaka City Metropolitan University, Osaka, Japan

Correspondence: Franziska Vielmuth, Vegetative Anatomy, Institute of Anatomy, Faculty of Medicine, Ludwig Maximilian University of Munich, Pettenkoferstraße 11, Munich 80336, Germany. E-mail: Franziska.Vielmuth@med.uni-muenchen.de

Abbreviations: AFM, atomic force microscopy; Ca^{2+}, calcium ion; Dp, desmoplakin; DSG, desmoglein; ECD, extracellular domain; KC, keratinocyte; KO, knockout; PV, pemphigus vulgaris; STED, stimulated emission depletion; WT, wild-type

Received 26 January 2023; revised 6 February 2024; accepted 2 March 2024; accepted manuscript published online 26 April 2024; corrected proof published online 21 June 2024

critically involved in the development of desmosomal hyper-adhesion and shows higher-order as well as higher single-molecule–binding strength under hyper-adhesive condition (Bartle et al, 2017; Fuchs et al, 2020). Desmosomal hyper-adhesion is highly regulated, and desmosomes are able to switch back to Ca^{2+} dependency, for example, to allow wound healing (Garrod et al, 2005; Kimura et al, 2007). In pemphigus, desmosomal hyper-adhesion was shown to protect from PV-IgG–induced loss of intercellular adhesion in vitro (Cirillo et al, 2010; Tucker et al, 2014). However, the mechanisms underlying this phenomenon are not yet elucidated. Thus, in this study, we analyzed single-molecule–binding properties of desmosomal cadherins under non-hyper-adhesive and hyper-adhesive conditions in pemphigus and investigated the effect of hyper-adhesion on PV-IgG–induced changes in DSG1 and DSG3 single-molecule–binding properties.

RESULTS

Hyper-adhesion protects KCs from PV-IgG–induced loss of intercellular adhesion and ameliorates DSG depletion and keratin retraction

To determine the timeline of acquisition of hyper-adhesion, we maintained KCs for 24–96 hours in high Ca^{2+} medium as suggested before (Garrod et al, 2005). Both murine and HaCaT human KCs revealed a spontaneously increasing adhesion between 24 and 96 hours in high Ca^{2+} medium (Supplementary Figure S1a and b). Importantly, during the same timeline, KCs acquired hyper-adhesiveness, as revealed by hyper-adhesion dissociation assays where the Ca^{2+} chelator EGTA was applied for 90 minutes to test for Ca^{2+} dependency (Garrod, 2013, 2005) (Figure 1a and Supplementary Figure S1c). In accordance, these time points were used as non-hyper-adhesive (24–36 hours) and hyper-adhesive (96 hours) throughout the study. In addition, under both adhesive conditions, DSG3 and desmoplakin (Dp) were present not only in desmosomes but also at the cell surface where the molecules are accessible for atomic force microscopy (AFM) adhesion measurements (Figure 1b). EGTA-mediated Ca^{2+} depletion led to a loss of DSG3 and Dp along cell contacts and on the cell surface under non-hyper-adhesive but not under hyper-adhesive condition, indicating that AFM accessible molecules also provide Ca^{2+}-independent characteristics (Figure 1b).

In pemphigus, hyper-adhesiveness was shown to influence autoantibody-induced loss of desmosomal adhesion in KCs (Cirillo et al, 2010; Tucker et al, 2014). In this study, application of both AK23, a pathogenic DSG3 antibody derived from a PV mouse model (Tsunoda et al, 2003), and PV2-IgG, containing pathogenic anti-DSG1 and -DSG3 antibodies, for 24 hours induced loss of intercellular adhesion in non-hyper-adhesive but not in hyper-adhesive murine KCs, confirming the protective effect of hyper-adhesiveness (Figure 1c and d).

DSG depletion and keratin retraction are morphological hallmarks of loss of intercellular adhesion in pemphigus, which progressively develop during autoantibody incubation (Oktarina et al, 2011; Schlögl et al, 2018; Waschke, 2008; Wilgram et al, 1961). Thus, we next investigated whether hyper-adhesion ameliorates these alterations. Under control condition, DSG1 and DSG3 were distributed linearly along cell borders in both non-hyper-adhesive and hyper-adhesive conditions. No changes in DSG3 or DSG1 membrane staining were observed after 1 hour incubation with PV2-IgG (Supplementary Figure S1d). Thus, the following AFM experiments were performed after 1 hour of autoantibody incubation to dissect the effects of direct inhibition from those caused by DSG depletion. 24 hours of incubation with PV2-IgG or AK23 led to depletion and fragmentation of DSG3 membrane staining in non-hyper-adhesive but not in hyper-adhesive murine KCs (Figure 1e and f and Supplementary Figure S2a and b). Similar results were observed for DSG1 after incubation with PV2-IgG (Supplementary Figure S1e and f). DSG depletion starts at the extradesmosomal pool of DSG molecules and progresses to DSG's in the desmosome-associated pool (Aoyama and Kitajima, 1999; Fuchs et al, 2023). To dissect DSG depletion of the respective pools, we used stimulated emission depletion (STED) microscopy and costained Dp as a desmosomal marker. Dp appeared as dots along the cell borders in non-hyper-adhesive murine KCs, whereas its membrane staining appears more linear under hyper-adhesive conditions (Figure 1g and Supplementary Figure S1g). The overall number and length of desmosomes, measured by Dp staining, were reduced after PV-IgG treatment in non-hyper-adhesive but not in hyper-adhesive KCs (Supplementary Figure S2c and d). DSG3/Dp colocalization was diminished after PV2-IgG treatment only in non-hyper-adhesive KCs, indicating a depletion of DSG3 from desmosomes (Figure 1g and h). In contrast, the overall stronger membrane coverage of DSG1 in hyper-adhesive KCs was slightly diminished by PV2-IgG (Supplementary Figure S1h). In addition, the amount of DSG3 along the cell membranes that was not colocalized to Dp and thus referred to as extradesmosomal was reduced only under non-hyper-adhesive condition (Figure 1g and Supplementary Figure S2e). STED microscopy of DSG1 staining revealed a fragmented membrane staining and reduced extra-desmosomal DSG1 solely in non-hyper-adhesive KCs (Supplementary Figures S1g and S2f).

A drastic change was also observed for the composition of the keratin cytoskeleton (cytokeratin 14 and cytokeratin 5) during acquisition of hyper-adhesion. Under non-hyper-adhesive condition, cytokeratins (CK) 5 and 14 built coarse, thick filaments, whereas a delicate and dense network was present in hyper-adhesive KCs (Figure 2a and b). PV2-IgG causes condensation of the filaments into less but thick bundles in non-hyper-adhesive KCs but barely induced changes under hyper-adhesive condition, confirmed by quantification of fluorescence intensity (Figure 2a and b and Supplementary Figure S3a and b). Taken together, these data demonstrate that hyper-adhesiveness ameliorates PV-IgG–induced DSG depletion and keratin retraction.

Hyper-adhesion did not alter accessibility of pathogenic autoantibodies to desmosomal cadherins

Hyper-adhesive desmosomes, in addition to Ca^{2+} independency, acquire an increased ordered ultrastructure, more ordered DSG3 distribution, and less mobile molecules (Fülle et al, 2021; Garrod et al, 2005). Thus, we asked whether these changes affect binding of pathogenic antibodies and thereby prevent loss of intercellular adhesion under

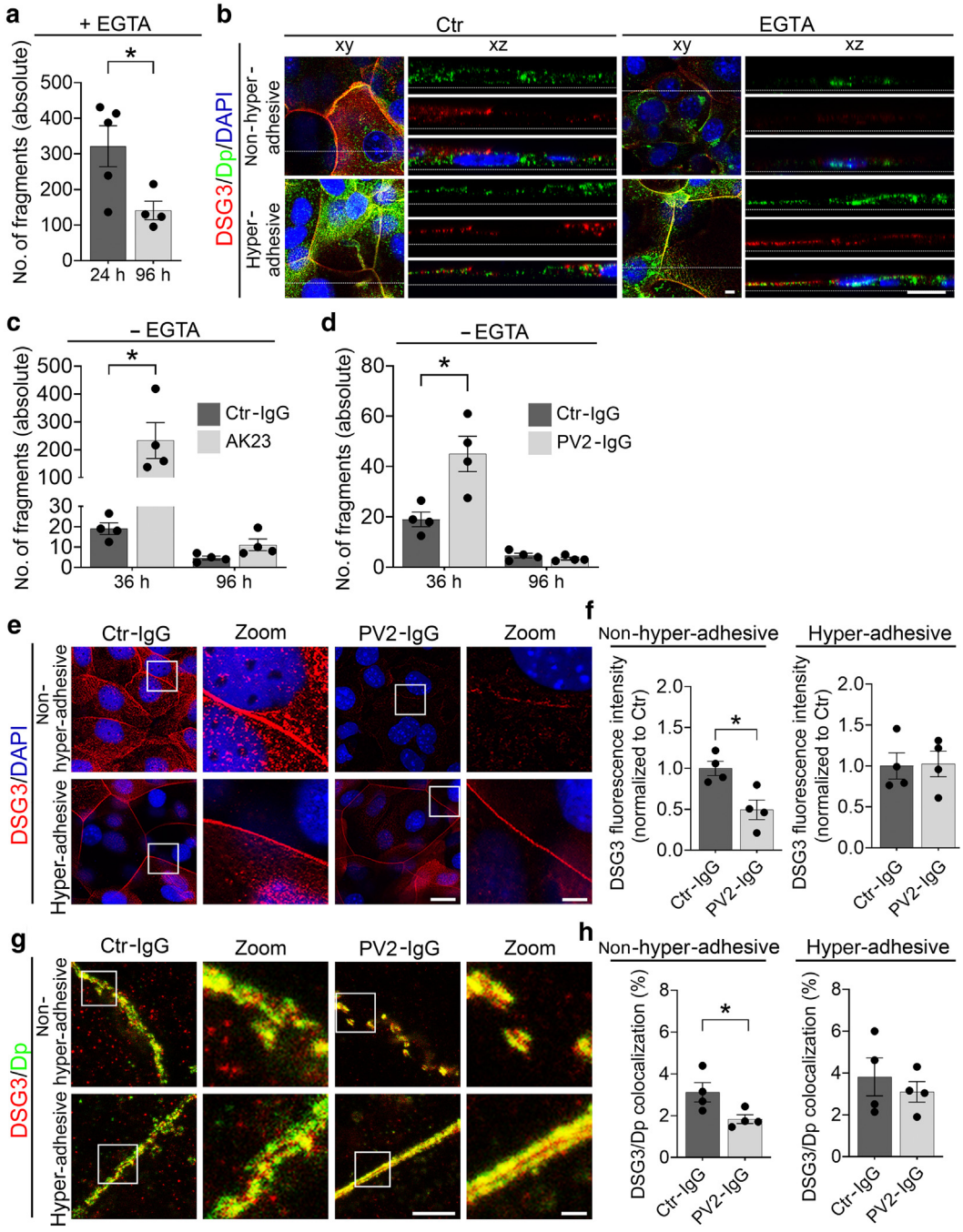

Figure 1. Hyper-adhesion protects KCs from PV-IgG–induced loss of intercellular adhesion and DSG depletion. (**a**) Hyper-adhesion dissociation assay with WT murine KCs. KCs incubated for 24 h in high-Ca^{2+} (1.2 mM) medium showed significantly more fragments than cells incubated for 96 h in high-Ca^{2+} medium ($n \geq 4$, mean ± SEM, $^*P < .05$). (**b**) Immunostaining of DSG3/Dp in non-hyper-adhesive (24 h in high-Ca^{2+} medium) and hyper-adhesive (96 h in high-Ca^{2+} medium) murine KCs. Both staining of DSG3 and Dp was significantly reduced after incubation of EGTA for 90 min in non-hyper-adhesive cells, whereas only a slight reduction of both proteins was observed in hyper-adhesive cells (representative $n \geq 4$). Bar xy = 10 μm and xz = 10 μm. (**c, d**) Dissociation assay under non-hyper-adhesive (36 h in high-Ca^{2+} medium) and hyper-adhesive (96 h in high-Ca^{2+} medium) conditions. (**c**) AK23 and (**d**) PV2-IgG incubation for 24 h prior to the experiment increased the number of fragments significantly in non-hyper-adhesive but not in hyper-adhesive murine KCs ($n = 4$, means ± SEM, $^*P < .05$; 2-way ANOVA with Bonferroni correction). (**e**) Immunostaining of DSG3 in non-hyper-adhesive (36 h in high-Ca^{2+} medium) and hyper-adhesive (96 h in high-Ca^{2+} medium) WT murine KCs. DSG3 revealed a continuous and linear membrane staining under control condition. PV2-IgG (24 h prior to experiment) led to a fragmented DSG3 membrane staining as well as reduced fluorescence intensity in non-hyper-adhesive but not in hyper-adhesive KCs (representative $n \geq 4$). Bar = 20 μm; zoom = 5 μm. (**f**) Quantification of DSG3 along cell borders in both states indicated a strong reduction only in non-hyper-adhesive cells ($n = 4$, means normalized to Ctr ± SEM, $^*P < .05$). STED analysis of DSG3/Dp costaining in murine KCs under the same condition reported in **g**. PV-IgG treatment led to a depletion of extradesmosomal DSG3 at sides of cell–cell contact (representative $n = 4$). Bar = 5 μm; zoom = 1 μm. (**h**) DSG3/Dp colocalization was reduced in non-hyper-adhesive but not in hyper-adhesive cells after PV2-IgG incubation for 24 h ($n = 4$, means ± SEM, $^*P < .05$). Ca^{2+}, calcium ion; Ctr, control; Dp, desmoplakin; DSG, desmoglein; h, hour; KC, keratinocyte; min, minute; PV, pemphigus vulgaris; STED, stimulated emission depletion microscopy; WT, wild-type.

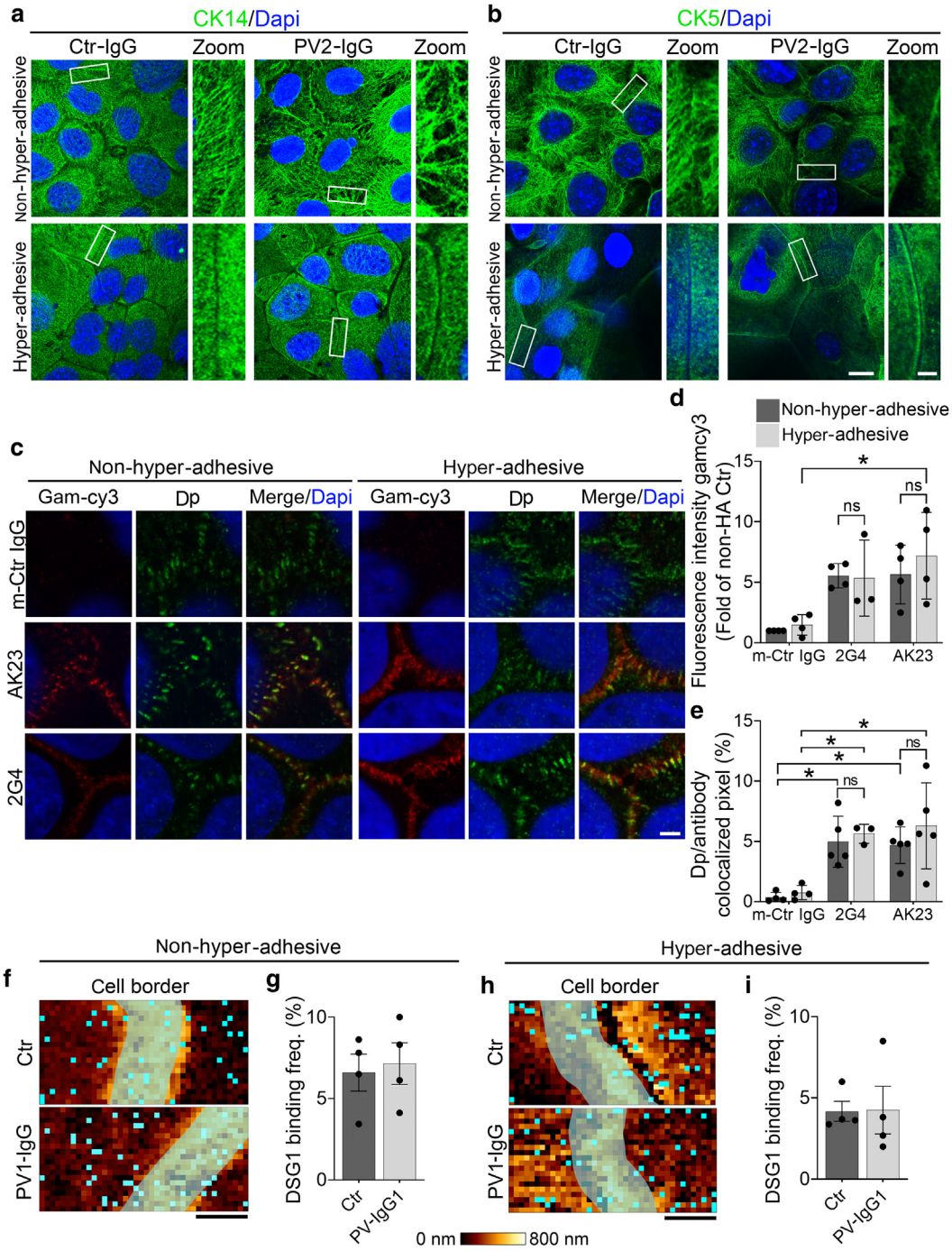

Figure 2. Hyper-adhesiveness ameliorates PV-IgG–induced alterations in the keratin cytoskeleton. (**a**) Immunostaining of CK14 in murine KCs revealed drastic changes in the composition of the keratin cytoskeleton between non-hyper-adhesive and hyper-adhesive cells. PV2-IgG led to retraction of the keratin cytoskeleton solely in non-hyper-adhesive KCs (representative n = 4) (bar = 20 μm; zoom = 5 μm). (**b**) CK5 immunostaining of non-hyper-adhesive murine KCs highlighted the strong changes in keratin architecture after 24-h incubation of PV2-IgG. The fine keratin meshwork of hyper-adhesive cells was not compromised (representative n = 4) (bar = 20 μm; zoom = 5 μm). (**c**) Immunostaining in non-hyper-adhesive and hyper-adhesive HaCaT cells revealed unchanged amount and distribution of bound AK23 and 2G4 in both adhesive cells states, (**d**) whereas almost no binding of Ctr-IgG was detected (representative n = 4) (bar = 3 μm) (n $\geq$ 3, means ± SEM, *$P < .05$; 2-way ANOVA with Bonferroni correction). (**e**) Colocalization analysis of bound antibody and Dp to dissect desmosome- from extradesmosomal-bound antibody showed for both adhesive conditions and both pathogenic anti-DSG3 comparable results (n $\geq$ 3, means ± SEM, *$P < .05$; 2-way ANOVA with Tukey's correction). (**f, h**) The 4 × 2 μm squares across cell borders were selected for DSG1 adhesion measurements. Cell borders were highlighted in white, whereas DSG1-binding events were displayed by cyan dots. (**g, i**) DSG1-binding frequency was unchanged in both adhesion states after incubation with PV1-IgG for 1 h (n = 4, from 4 independent coating procedures, 2 cell border adhesion maps with 800 force–distance curves/adhesion map, means ± SEM, *$P < .05$). Bar = 1 μm. CK14, cytokeratin 14; CK5, cytokeratin 5; Ctr, control; Dp, desmoplakin; DSG, desmoglein; h, hour; KC, keratinocyte; PV, pemphigus vulgaris.

hyper-adhesive condition. Therefore, we incubated pathogenic anti-DSG3 antibodies targeting several parts of the DSG3 ECD for 1 hour. In detail, we applied AK23, targeting the binding pocket of the ECD1 of DSG3 (Tsunoda et al, 2003), and 2G4, targeting the membrane proximal ECD5 of DSG3 (amino acid 451−566) (Hudemann et al, 2023) in human KCs (Figure 2c), as well as PV2-IgG, containing a polyclonal batch of anti-DSG3 antibodies, in murine KCs (Supplementary Figure S3c). Interestingly, detection of bound AK23, PV2-IgG, and 2G4 depicted the same fluorescence intensity and therefore binding to DSG3 in the membrane under both adhesive states in the respective cell line (Figure 2c and d and Supplementary Figure S3c and d). In addition, antibody binding colocalized to Dp was not changed in both adhesive states (Figure 2e and Supplementary Figure S3e), indicating no changes in the ratio of desmosome- versus extradesmosomal-bound antibodies. Thus, protective effects of hyper-adhesiveness in pemphigus were not caused by changes in antibody binding.

Previous data reported that DSG-binding properties change during acquisition of hyper-adhesiveness (Fuchs et al, 2020). Thus, we next analyzed desmosomal cadherin−binding frequency in both adhesive states. Murine KCs had a slightly increased binding frequency in non-hyper-adhesive compared with that in hyper-adhesive KCs for DSG1, DSG3, and DSC3, suggesting that less molecules were accessible for AFM measurements (Supplementary Figure S3f and g). Importantly, levels were clearly above measurements from tips coated with hFc fragment, which were used to determine the amount of unspecific binding events (Supplementary Figure S4a). Furthermore, results for the respective desmosomal cadherins were analyzed by Poisson statistic, which predicted 94−98% probability of measuring single-molecule interactions (Supplementary Figure S4b).

Hyper-adhesion does not change DSG1-binding properties

Previous experiments showed that homophilic DSG1 interactions are not affected by pemphigus autoantibodies−induced direct inhibition but caused DSG1 redistribution (Hiermaier et al, 2022; Vielmuth et al, 2018b; Waschke et al, 2005). To investigate whether hyper-adhesion influences this phenomenon, we performed AFM DSG1 adhesion measurements on living murine KCs. Importantly, surface topography of murine KCs with elevated cell borders revealed no drastic changes between the 2 adhesive states (Supplementary Figure S4c) (Vielmuth et al, 2018c). For all further adhesion measurements, small areas along cell borders were chosen. Antibodies were solely incubated on the measured cells, and cells were extensively washed to remove unbound antibody to avoid antibody binding to the molecules coated on the scanning tip. In adhesion maps, each pixel represents 1 force−distance curve, and each cyan pixel represents 1 specific DSG1-binding event (Figure 2f and h). In accordance with previous studies (Vielmuth et al, 2018a, 2018b; Waschke et al, 2005), PV1-IgG application for 1 hour did not affect DSG1 single-molecule−binding frequency (Figure 2g and i), confirming that direct inhibition does not occur for DSG1-mediated binding events. In addition, DSG1-unbinding forces (Supplementary Figure S4d) remain unaltered in both adhesive states, indicating that changes in DSG1-binding properties do not account for protective effects of hyper-adhesiveness. Thus, we subsequently focused on direct inhibition of DSG3-mediated interactions.

Hyper-adhesion reduces susceptibility to direct inhibition of DSG3 interactions in dependency on the autoantibody-binding epitope

In contrast to DSG1, DSG3 interactions are directly inhibited upon PV-IgG binding (Heupel et al, 2008; Vielmuth et al, 2018b, 2015; Waschke et al, 2005), and hyper-adhesion strengthens DSG3 single-molecule interactions (Fuchs et al, 2020). Thus, we next checked for direct inhibition of DSG3 interactions under both adhesive states.

First, PV2-IgG was used, which contains polyclonal autoantibodies putatively directed against several parts of the DSG3 ECD (Figure 3a) (Amagai et al, 1992; Müller et al, 2008; Sekiguchi et al, 2001). Under control condition, DSG3-binding events were uniformly distributed along the small areas along cell borders chosen for adhesion measurements (Figure 3b). Importantly, PV2-IgG incubation led to a significant direct inhibition in non-hyper-adhesive but not in hyper-adhesive KCs (Figure 3b and c). In contrast, PV2-IgG incubation had no effect on the remaining unbinding forces (Supplementary Figure S4e). PV sera contain a polyclonal mixture of DSG3-specific IgG antibodies (Aksu et al, 2010; Weiss et al, 2015). Thus, we wondered whether antibodies targeting several parts of the DSG3 ECD differ in their potential to induce direct inhibition under certain adhesive states and selected well-characterized antibodies that bind to different epitopes of the DSG3 ECD (Supplementary Figure S4f). AFM experiments were performed on HaCaT human KCs. The topography of HaCaTs did not change significantly between both adhesive states (Supplementary Figure S5a). In this study, we compared 2 pathogenic antibodies targeting the 2 opposing ends of the DSG3 ECD: AK23 and 2G4 (Figure 3d and g and Supplementary Figure S4f). Surprisingly, 1 hour incubation of AK23 directly inhibited DSG3 interactions in non-hyper-adhesive and strongly in hyper-adhesive HaCaT cells (Figure 3e and f). In contrast, 1 hour incubation of 2G4 induced direct inhibition of DSG3 interactions only in non-hyper-adhesive HaCaT cells (Figure 3h and i). To confirm these results in murine KCs, we repeated the experiments with AK23 and the commercially available antibody 5G11, directed against the ECD5, which confirmed the epitope-specific direct inhibition by pathogenic antibodies under hyper-adhesive condition (Figure 3j−l and Supplementary Figure S5b and c). The unbinding forces of the remaining events were unaffected in both adhesive conditions and with both antibodies (Supplementary Figure S5d−f).

Taken together, these data indicate that the binding epitope of pathogenic autoantibodies defines their capacity to induce direct inhibition under hyper-adhesive condition and thus suggest that the DSG3 interaction mechanisms differ between non-hyper-adhesive and hyper-adhesive conditions. Importantly, they also show that mechanisms other than direct inhibition are crucial for loss of intercellular adhesion in pemphigus because AK23 induces direct inhibition under hyper-adhesive condition, although they are protected from loss of intercellular adhesion.

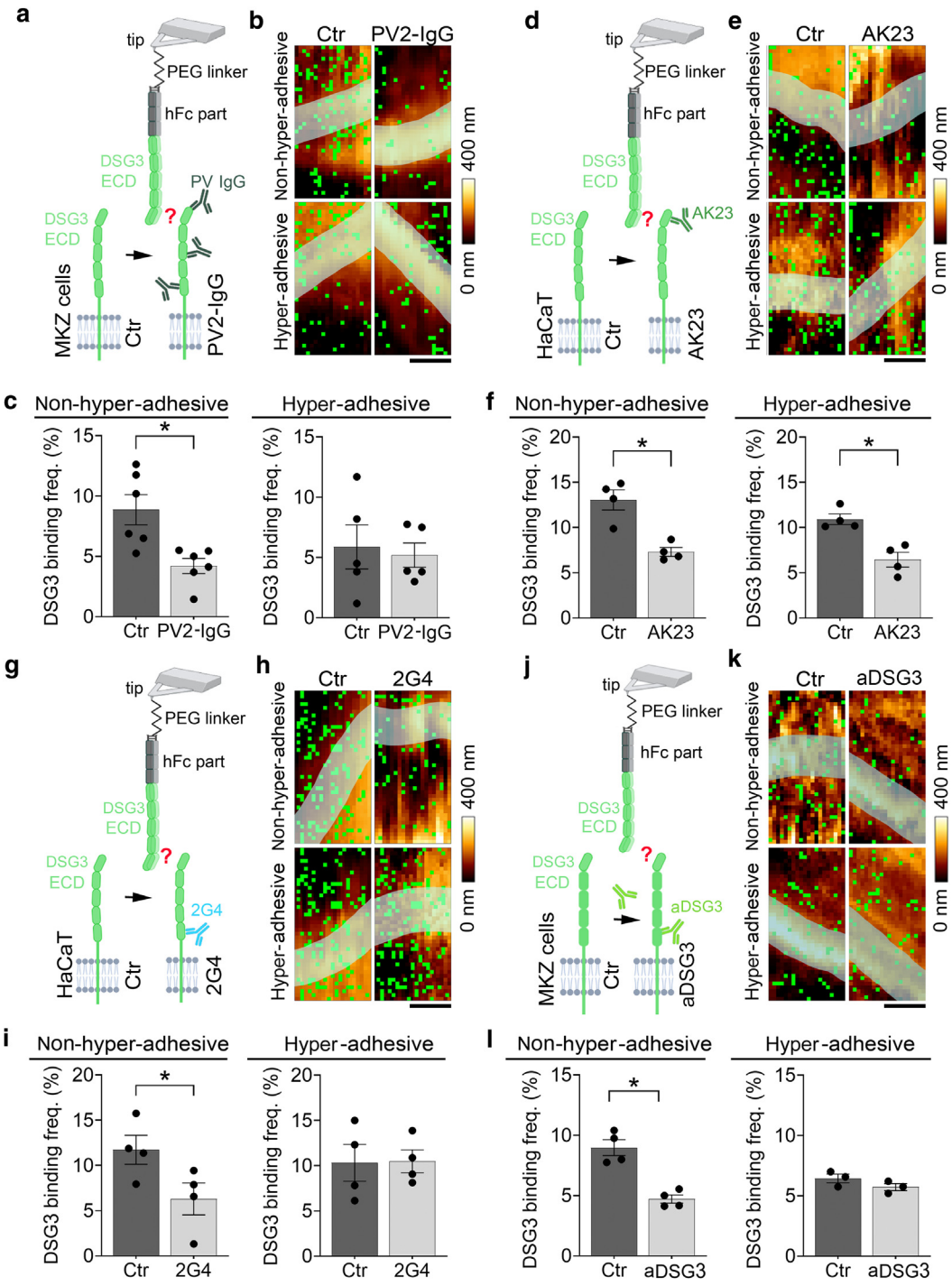

Figure 3. Hyper-adhesion prevents DSG3-direct inhibition in an epitope-dependent manner. (**a**) Schematic of AFM measurement with DSG3-coated tip. Polyclonal PV2-IgGs bind multiple epitopes of DSG3 and were solely incubated on the cells to avoid antibody binding to the scanning tip. (**b**) AFM adhesion maps for DSG3 of cell borders of murine KCs under non-hyper-adhesive (24 h in high-Ca^{2+} medium) and hyper-adhesive (96 h in high-Ca^{2+} medium) conditions. Every green dot represents 1 DSG3-dependent binding event. Cell borders are highlighted in white. PV2-IgG incubation for 1 h led to a drastic reduction in binding frequency in non-hyper-adhesive but not in hyper-adhesive KCs. Bar = 1 μm. (**c**) Quantification of DSG3-binding frequency delineated a significant direct inhibition of DSG3 interactions only in non-hyper-adhesive murine KCs when incubated with PV2-IgG for 1 h ($n \geq 5$, from 5 independent coating procedures, 2 cell border adhesion maps with 800 force–distance curves/adhesion map, means ± SEM, $^*P < .05$). (**d**) Schematic of AFM measurement with DSG3-coated tip. AK23, a murine monoclonal anti-DSG3 antibody, binds specifically to the ECD1 of DSG3 and was solely incubated on the cells to avoid antibody binding to the scanning tip. (**e**) AFM DSG3 adhesion maps of HaCaTs. Bar = 1 μm. AK23 incubation for 1 h led to a significant decrease in DSG3-binding frequency in both adhesive states. (**f**) Quantification of DSG3-binding frequency showed a significant direct inhibition in both adhesive states after treatment with AK23 (n = 4 from 4 independent coating procedures, 800 force–distance curves/adhesion map, means ± SEM, $^*P < .05$). (**g**) Schematic of AFM measurement with DSG3-coated tip. The antibody 2G4, a murine monoclonal anti-DSG3 antibody, binds specifically on the ECD5 and was solely incubated on the cells to avoid antibody binding to the scanning tip. (**h**) AFM adhesion maps of HaCaTs for DSG3 as described earlier. The 2G4 incubation for 1 h led to a decrease in DSG3-binding frequency only in non-hyper-adhesive KCs. Bar = 1 μm. (**i**) Quantification of DSG3-binding frequency revealed a significant direct inhibition in non-hyper-adhesive murine KCs only (n = 4 from 4 independent coating procedures, 800 force–distance curves/adhesion map, means ± SEM,

Hyper-adhesion ameliorates antibody-induced DSC3 alterations and reduces susceptibility to direct inhibition of DSC3 interactions

Autoantibodies against DSC3 were reported to be pathogenic in a subset of patients with pemphigus (Mao et al, 2010; Rafei et al, 2011; Spindler et al, 2009). Similar to previous results, 24 hour incubation with the monoclonal anti-DSC3 antibody (clone U114, Progen) led to a drastic loss of intercellular adhesion in non-hyper-adhesive but only a slight fragmentation in hyper-adhesive murine KCs (Figure 4a and Supplementary Figure S6a). In accordance, non-hyper-adhesive but not hyper-adhesive KCs, treated for 24 hours with anti-DSC3, depict a fragmented and reduced DSC3 staining along cell borders (Supplementary Figure S6b and c). Furthermore, DSC3 and Dp double staining in STED experiments revealed that DSC3/Dp colocalization was reduced under non-hyper-adhesive but not under hyper-adhesive condition (Figure 4b and Supplementary Figure S6e). Furthermore, extradesmosomal DSC3 was depleted solely in non-hyper-adhesive KCs (Supplementary Figure S6d).

Next, we characterized changes in DSC3 single-molecule–binding frequency after incubation with an anti-DSC3 antibody, targeting the DSC3 ECD5 (Figure 4c). In accordance, to epitope the dependency of direct inhibition in DSG3, the anti-DSC3 antibody blocked interactions in non-hyper-adhesive but not in hyper-adhesive cells (Figure 4d and e). The unbinding force of the remaining binding events slightly increased after treatment with anti-DSC3 (Supplementary Figure S6f). These data indicate that susceptibility to direct inhibition is comparable for DSG3 and DSC3, and thus changes in the interaction mechanisms between non-hyper-adhesive and hyper-adhesive KCs may be comparable for DSG3 and DSC3.

Reduced susceptibility of DSG3 interactions to direct inhibition is not caused by heterophilic interactions to DSC3 or DSG2

Homophilic and heterophilic interactions and their contributions to pemphigus pathogenesis remain controversially discussed (Harrison et al, 2016; Ishii et al, 2020; Vielmuth et al, 2018c). To investigate whether changes in direct inhibition are caused by distinct interaction partner of DSG3 under certain adhesive states, for example, a switch to heterophilic interactions such as DSG3–DSC3 or DSG3–DSG2, we performed DSG3 adhesion measurement and applied antibodies specific for individual desmosomal cadherin isoforms (Supplementary Figure S4f provides more details about binding epitopes).

First, an anti-DSC3 was applied solely on the cells, and DSG3 adhesion measurements were performed thereafter (Figure 4f). However, the anti-DSC3 antibody had no effect on DSG3-binding frequency in non-hyper-adhesive and hyper-adhesive KCs, suggesting that predominantly homophilic DSG3 but not heterophilic DSG3–DSC3 interactions are present (Figure 4g and Supplementary Figure S7a). In accordance, DSG3-unbinding forces also remained unaltered (Supplementary Figure S7b). Vice versa, we applied AK23 on murine KCs and performed DSC3 AFM adhesion measurements (Figure 4h). In accordance with the previous experiments, we did not observe an effect of AK23 on DSC3-dependent interactions, and thus heterophilic DSC3–DSG3 interactions seem to be less abundant or absent in both adhesive states in murine KCs (Figure 4i and Supplementary Figure S7c and d).

Previously, AFM data reported heterophilic interactions of DSG2 and DSG3 (Sigmund et al, 2020; Vielmuth et al, 2018c). Thus, we next applied a commercially available anti-DSG2 antibody, targeting the ECD2–3 of DSG2 (Ori-Gene Technologies) (Supplementary Figure S7e), which was shown previously to block homophilic DSG2–DSG2 and heterophilic DSG2–DSG3 interactions (Vielmuth et al, 2018c). DSG3 adhesion measurements revealed no changes in DSG3-binding frequency under both adhesive states (Supplementary Figure S7f), indicating that heterophilic DSG2–DSG3 interactions are absent or only present to a minor extent under both adhesive conditions. Taken together, these data suggest that predominantly homophilic DSG3 interactions were measured under both adhesive states, and thus changes in direct inhibition were not caused by altered interaction partners of DSG3.

DSG3 loss modulates DSC3-binding properties and induces a compensatory DSG2 upregulation

DSG3 was shown to be involved in acquisition of desmosomal hyper-adhesion (Fuchs et al, 2020). Thus, we next performed experiments using murine DSG3-knockout (KO) KCs (Koch et al, 1997). DSG3-KO KCs revealed reduced hyper-adhesiveness after 96 hours of differentiation (Figure 5a). Immunofluorescence staining in wild-type (WT) and DSG3-KO KCs incubated 24 and 96 hours of Ca^{2+} showed a membrane staining of DSG2 in both adhesive states only in DSG3-KO cells, whereas DSC3 staining remained unaltered (Supplementary Figure S7g). Next, we used the 5G11 mAb against DSG3 in DSG3-KO KCs (Supplementary Figure S8a). As expected, the antibody had no effect on binding frequency when the cells were measured with a DSG3-coated tip (Supplementary Figure S8b), demonstrating that the antibody specifically bound DSG3.

To check whether an interplay of DSG3 and DSC3 is important for hyper-adhesion, we performed KC dissociation assays on DSG3-KO murine KCs with an anti-DSC3 antibody. In contrast to WT KCs, the anti-DSC3 antibody induced fragmentation after 24 and 96 hours of Ca^{2+} differentiation (Figure 5b), underlining the importance of DSG3 for acquisition of desmosomal hyper-adhesion. Next, we used the anti-DSC3 antibody in DSC3 AFM adhesion measurements.

$^*P < .05$). (**j**) Schematic of AFM measurement with DSG3-coated tip. A commercially available anti-DSG3 antibody (5G11) binds specifically on the ECD5 domain and was solely incubated on the cells to avoid antibody binding to the scanning tip. (**k, l**) Adhesion measurements of WT murine KCs incubated with the anti-DSG3 mAb 5G11 revealed a reduction of the DSG3-binding frequency only in non-hyper-adhesive (24 h in high-Ca^{2+} medium) cells. Bar = 1 μm (n = 4, from 4 independent coating procedures, 2 cell border adhesion maps with 800 force–distance curves/adhesion map, means ± SEM, $^*P < .05$). AFM, atomic force microscopy; Ca^{2+}, calcium ion; Ctr control; DSG, desmoglein; ECD, extracellular domain; h, hour; KC, keratinocyte; PEG, polyethylene glycol; PV, pemphigus vulgaris; WT, wild-type.

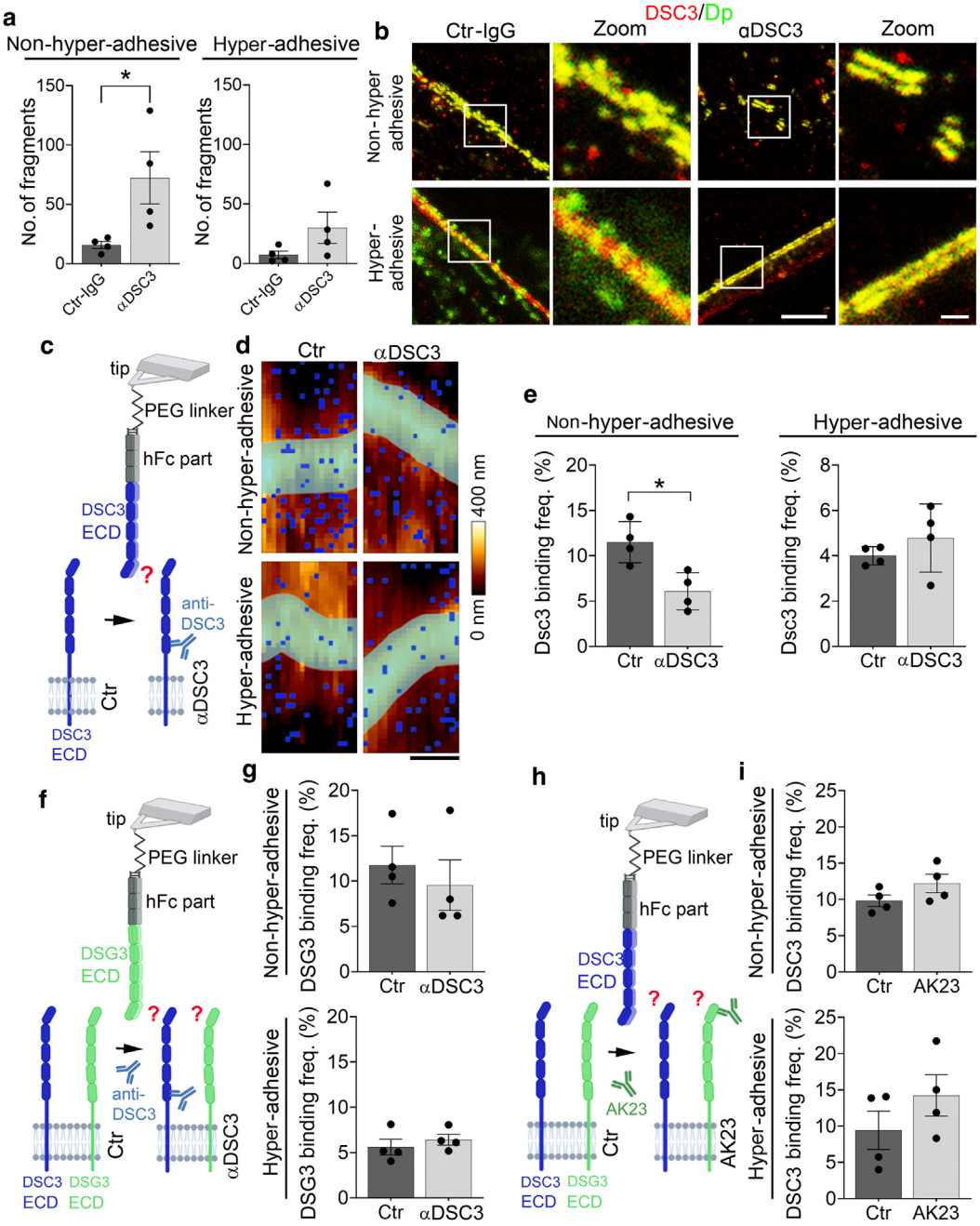

Figure 4. Changes in susceptibility to autoantibody-induced direct inhibition are not caused by a shift from homophilic to heterophilic interactions. (**a**) Dissociation assay in WT murine KCs revealed that only non-hyper-adhesive (36 h in high-Ca^{2+} medium) cells showed a significant loss of KC cohesion after application of a monoclonal anti-DSC3 antibody for 24 h (n = 4, means ± SEM, *$P < .05$). (**b**) STED analysis of DSC3/Dp costaining in WT murine KCs showed a decrease of extradesmosomal DSC3 after incubation with PV2-IgG for 24 h, especially in non-hyper-adhesive (36 h in high-Ca^{2+} medium) KCs. In addition, an anti-DSC3 antibody induced a fragmented membrane DSC3 staining (n = 4). Bar = 5 μm; zoom = 1 μm. (**c**) Schematic of AFM measurement with DSC3-coated tip. The monoclonal anti-DCS3 antibody targets the ECD5 of DSC3 and was solely incubated on the cells to avoid antibody binding to the scanning tip. (**d**) AFM DSC3 adhesion maps of non-hyper-adhesive (24 h in high-Ca^{2+} medium) and hyper-adhesive (96 h in high-Ca^{2+} medium) murine KCs. Topography images revealed elevated cell borders (marked in lighter color). Every blue dot represents a specific DSC3-dependent binding event. Incubation with DSC3 antibody for 1 h induced a decrease in binding frequency in non-hyper-adhesive (24 h in high-Ca^{2+} medium) but not in hyper-adhesive (96 h in high-Ca^{2+} medium) KCs. Bar = 1 μm. (**e**) Quantification of DSC3-binding frequency showed a significant direct inhibition only in non-hyper-adhesive murine KCs (n = 4, from 4 independent coating procedures, 2 cell border adhesion maps with 800 force–distance curves/adhesion map, means ± SEM, *$P < .05$). (**f**) Schematic of AFM measurement with DSG3-coated tip. The monoclonal anti-DCS3 antibody targets the ECD5 of DSC3 and was solely incubated on the cells to avoid antibody binding to the scanning tip. (**g**) The DSC3 antibody induced no changes in the DSG3-binding frequency in WT murine KCs (n = 4, from 4 independent coating procedures, 2 cell border adhesion maps with 800 force–distance curves/adhesion map, means ± SEM, *$P < .05$). (**h**) Schematic of AFM measurement with DSC3-coated tip. AK23 targets the ECD1 of DSG3 and was solely incubated on the cells to avoid antibody binding to the scanning tip. (**i**) The frequency was unchanged after application of AK23 for 1 h (n = 4, from 4 independent coating procedures, 2 cell border adhesion maps with 800 force–distance curves/adhesion map, means ± SEM, *$P < .05$). AFM, atomic force microscopy; Ca^{2+}, calcium ion; Ctr, control; Dp, desmoplakin; DSG, desmoglein; ECD, extracellular domain; h, hour; KC, keratinocyte; PEG, polyethylene glycol; PV, pemphigus vulgaris; STED, stimulated emission depletion; WT, wild-type.

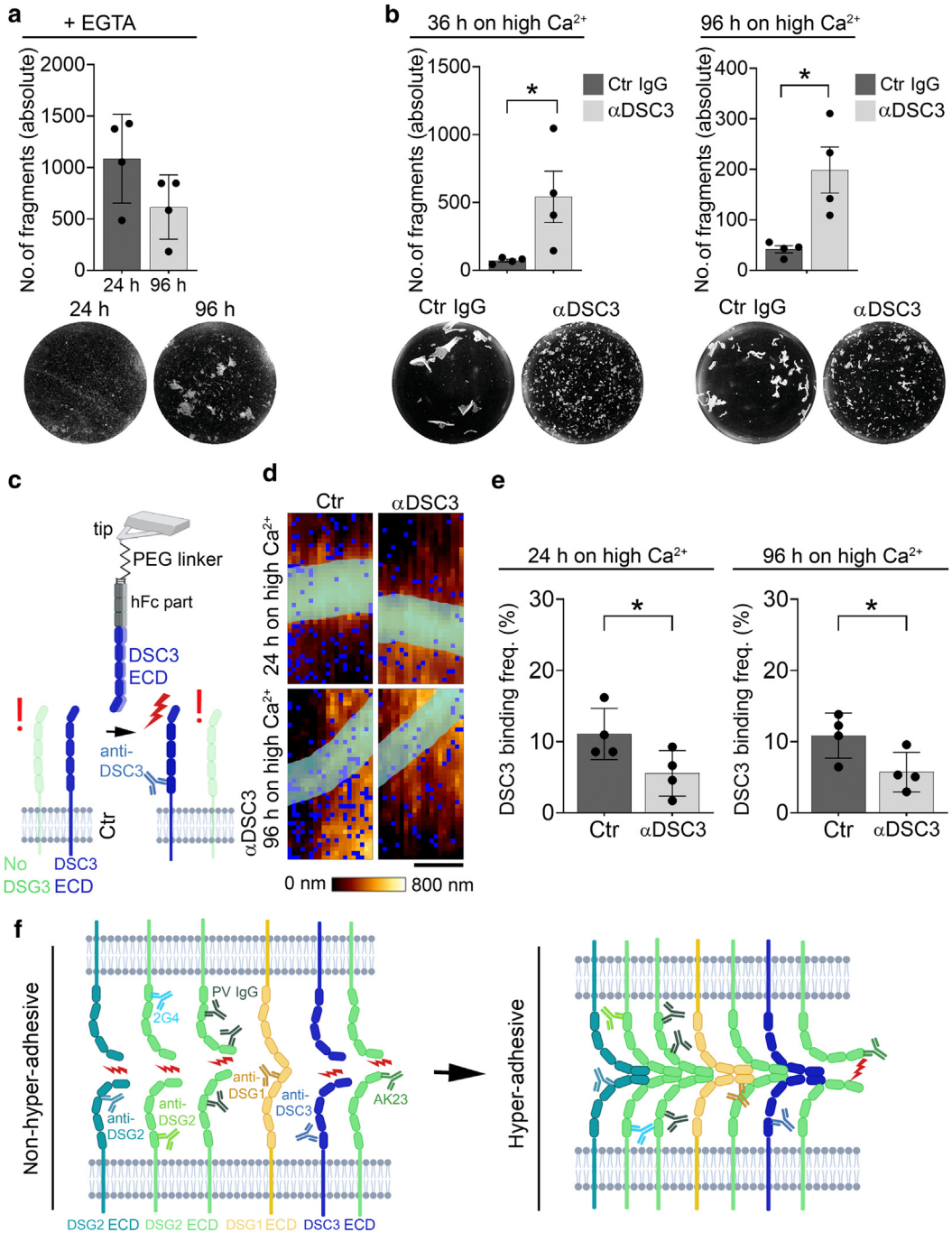

Figure 5. DSG3-KO murine KCs do not reach hyper-adhesiveness. (**a**) Hyper-adhesion dissociation assay with DSG3-KO murine KCs. No significant differences of fragment number between cells incubated for 36 h and KCs incubated for 96 h in high-Ca^{2+} medium (n = 4, means ± SEM, *$P < .05$). (**b**) Dissociation assay with DSG3-KO murine KCs showed that the anti-DSC3 antibody strongly fragmented cell monolayers of both times points, whereas Ctr-IgG showed almost no fragments in both adhesion states (n = 4, means ± SEM, *$P < .05$). (**c**) Schematic of AFM measurement with DSC3-coated tip. The anti-DSC3 antibody directly inhibit DSC3 interaction on the ECD5 and was solely incubated on the cells to avoid antibody binding to the scanning tip. (**d**) DSC3-binding frequency was analyzed in DSG3-KO murine KCs cultivated for 36 and 96 h in high-Ca^{2+} medium. AFM DSC3 adhesion maps from 2 different time points across the cell border area of 2 adjacent cells showed that anti-DSC3 incubation for 1 h directly inhibited binding events (represented by blue dots) of both states of adhesion. Bar = 1 μm. (**e**) Quantification of DSC3-binding frequency revealed that cells cultivated for 24 h in high-Ca^{2+} medium as well as KCs cultivated for 96 h in high-Ca^{2+} medium had a drastic reduction of the DSC3-binding frequency after treatment with the anti-DSC3 antibody (n = 4, from 4 independent coating procedures, 2 cell border adhesion maps with 800 force–distance curves/adhesion map, means ± SEM, *$P < .05$). (**f**) Schematic of direct inhibition of DSG and desmocollin interactions in both adhesive states. AFM, atomic force microscopy; Ca^{2+}, calcium ion; Ctr, control; DSG, desmoglein; ECD, extracellular domain; h, hour; KC, keratinocyte; KO, knockout.

In accordance to the previously mentioned KC dissociation assay, the anti-DSC3 antibody induced direct inhibition in both 24- and 96-hour Ca^{2+}-differentiated KCs (Figure 5c–e). In addition, unbinding force of DSC3 interactions in DSG3-KO KCs did not change during differentiation or treatment (Supplementary Figure S8c), indicating that binding

properties of DSC3 remain comparable if cells do not become hyper-adhesive because of DSG3 deficiency.

Compromised DSG3-mediated adhesion in KCs is partly compensated by an upregulation of DSG2 and heterophilic DSG2−DSG3 interactions (Hartlieb et al, 2014; Sigmund et al, 2020; Vielmuth et al, 2018c). Thus, we next applied an anti-DSG2 antibody and measured DSG3-mediated adhesion in DSG3-KO KCs. Indeed, we observed that in contrast to WT KCs, where an anti-DSG2 antibody (OriGene) had no effect on DSG3-mediated adhesion in both adhesive states (Supplementary Figure S7e and f), the antibody was capable of blocking interactions measured with a DSG3-coated tip, indicating that more DSG2 is present along the cell membrane, and thus, heterophilic DSG2−DSG3 interactions occurred (Supplementary Figure S8d). Fitting to the epitope-specific ability to cause direct inhibition, the antibody targeting the ECD2 and ECD3 reduced binding frequency but not to a significant extent under hyper-adhesive condition (Supplementary Figure S8e).

Taken together, these data underline the importance of DSG3 for acquisition of hyper-adhesion and showed that DSG3 also influences the susceptibility of other molecules, such as DSC3, to autoantibody-induced direct inhibition. In addition, expression of desmosomal cadherin isoforms, such as DSG2 and DSG3, is interdependent, and a compensatory upregulation of DSG2 occured under non-hyper-adhesive and hyper-adhesive conditions.

DISCUSSION

Desmosomal hyper-adhesion was suggested to be protective against loss of intercellular adhesion in pemphigus, although the underlying mechanisms are largely unknown. Our data showed that desmosomal hyper-adhesion ameliorates PV-IgG−induced DSG depletion as well as keratin retraction. Furthermore, we found that hyper-adhesion reduces susceptibility to autoantibody-mediated direct inhibition of DSG3 interactions in an epitope-dependent manner and show that mechanistically, neither changes in autoantibody binding nor in interaction partners of DSG3 account for this phenomenon. Furthermore, the data demonstrate that mechanisms other than direct inhibition of DSG3 interactions are crucial for sufficient loss of intercellular adhesion in pemphigus.

Hyper-adhesion protects KCs from PV-IgG−induced loss of intercellular adhesion

A unique property of desmosomes is their ability to confer strong cohesion and high plasticity by maturing from a weak to a stronger adhesive state, described as hyper-adhesion (Garrod et al, 2005; Kimura et al, 2007). In accordance with previous studies, we observed a protective effect of hyper-adhesion (Cirillo et al, 2010) with diminished PV-IgG−induced DSG and DSC depletion and keratin retraction in hyper-adhesive KCs, both of which are morphological hallmarks in pemphigus and correlate with loss of KC cohesion (Aoyama and Kitajima, 1999; Berkowitz et al, 2005; Schlögl et al, 2018). Interestingly, the keratin cytoskeleton undergoes substantial changes during acquisition of hyper-adhesion. Importantly, AK23 induced direct inhibition of DSG3 interactions under both adhesive states, although hyper-adhesive KCs were protected from AK23-induced loss of intercellular adhesion, showing that mechanisms other than direct inhibition are important for development of a pemphigus phenotype. This is consistent with previous data, showing that direct inhibition alone is not sufficient for loss of intercellular adhesion in pemphigus and delineating the importance of signaling pathways in pemphigus pathogenesis (Spindler et al, 2018; Spindler and Waschke, 2014; Vielmuth et al, 2015).

Hyper-adhesion reduces susceptibility to PV-IgG−induced direct inhibition of DSG3 interactions in an epitope-dependent manner

Among the mechanisms leading to loss of KC cohesion in pemphigus, autoantibodies cause direct inhibition of DSG3 but not of DSG1 interactions (Heupel et al, 2008; Spindler et al, 2009; Waschke et al, 2005). For all AFM experiments, 1 hour incubation with pathogenic antibodies was used. In accordance with previous studies, levels of desmosomal cadherins along the plasma membrane were unaltered at this time point, and thus observed effects on binding probability can be ascribed to direct inhibition (Schlögl et al, 2018; Vielmuth et al, 2015).

Surprisingly, PV2-IgG inhibits DSG3 interactions in non-hyper-adhesive cells only. PV-IgGs are polyclonal antibodies directed against several parts of the ECD of DSG3 (Dworschak et al, 2012). Although previous data indicate that pathogenicity of autoantibodies targeting the ECD1 and ECD2 is highest, also antibodies targeting other parts of the ECD can also cause intraepidermal loss of adhesion (Hudemann et al, 2023; Müller et al, 2006). Recently, epitope-specific signaling was observed for DSG3 (Schmitt et al, 2023). In this study, we observed that AK23 binding the N-terminal region of DSG3 inhibits DSG3 interaction in both adhesive states, whereas 2G4, a pathogenic antibody (Hudemann et al, 2023), and 5G11, both targeting the membrane-proximal region of DSG3, were capable of inducing direct inhibition in non-hyper-adhesive KCs only. This difference is not caused by changes in accessibility to membrane-proximal autoantibody-binding sites as revealed by immunostainings. However, conformational changes of the ECD, organization of desmosomal cadherins at desmosome, as well as changes in clustering and molecule mobility may be more important (Figure 5f) (Bartle et al, 2020; Beggs et al, 2022; Fuchs et al, 2020; Fülle et al, 2021; Hatzfeld et al, 2000). Thus, reduced direct inhibition under hyper-adhesive condition may also be caused by a different interaction mechanism of desmosomal cadherins in dependency on the adhesive state, which was indicated before for DSG3, by higher unbinding forces under hyper-adhesive condition (Figure 5f) (Fuchs et al, 2020).

Homophilic interactions of DSG3 are predominant under both adhesive conditions

Desmosomal cadherins undergo homophilic and heterophilic interactions (Harrison et al, 2016; Lowndes et al, 2014a; Vielmuth et al, 2018a). Previous studies have shown that heterophilic interactions also occur between DSG2−DSC2 or DSG2 and the classic cadherins E-cadherin and N-cadherin where the data indicate that the respective interaction mechanisms may differ (Fuchs et al, 2022;

Lowndes et al, 2014b; Shafraz et al, 2018). In addition, we recently identified that heterophilic DSG2−DSG3 interactions may occur in pemphigus and serve as a rescue mechanism (Sigmund et al, 2020). Thus, one can speculate that changes in the susceptibility to PV-IgG−induced direct inhibition are due to distinct interaction partners under non-hyper-adhesive versus hyper-adhesive conditions. Previous data report that PV-IgG induce direct inhibition of heterophilic DSG3−DSC3 interaction in bead assays (Ishii et al, 2020) and a compensatory upregulation of DSG2 that may be beneficial by heterophilic DSG2−DSG3 interactions (Sigmund et al, 2020). However, AFM data in this study did not detect predominant heterophilic transinteractions of DSG3−DSC3 or DSG3−DSG2 in WT KCs but demonstrate direct inhibition of homophilic DSG3−DSG3 or DSC3−DSC3 by respective antibodies. However, although less likely, further heterophilic interactions cannot be ruled out by this study and may require further investigation, especially because previous studies found that desmosomal cadherins undergo homophilic and heterophilic interactions with, among others, certain classical cadherins and further membrane proteins such as the EGFR (Fuchs et al, 2022; Harrison et al, 2016; Ishii et al, 2020; Ungewiss et al, 2018; Vielmuth et al, 2018a).

Data on DSG3-KO murine KCs, which fail to become hyper-adhesive, show that the presence of DSG3 is important to acquire and maintain hyper-adhesion. Importantly, DSG3-KO murine KCs could not prevent the loss of cell cohesion caused by a pathogenic anti-DSC3 antibody. This is in line with previous data showing that desmosomal cadherins differently contribute to hyper-adhesion (Fuchs et al, 2019).

Conclusively, reduced susceptibility to PV-IgG−induced direct inhibition under hyper-adhesive condition may contribute to protective effects of hyper-adhesion in pemphigus and reveals insights into distinct interactions modes of desmosomal cadherins under certain biological conditions.

MATERIALS AND METHODS

For extended materials and methods, please also refer to Supplementary Materials and Methods.

Cell culture

WT murine KCs were cultivated in low-calcium complete FAD media (0.05 mM calcium chloride, PAN Biotech) on collagen I (rat tail) as previously described (Fuchs et al, 2020; Sigmund et al, 2020). To induce differentiation, confluent murine KCs were switched to high Ca^{2+}-containing medium (1.2 mM). HaCaT cells are a kind gift from Petra Boukamp (German Cancer Research Center, Heidelberg, Germany) and cultivated in DMEM (Life Technologies) containing 1.8 mM Ca^{2+} supplemented with 10% fetal bovine serum (Sigma-Aldrich), 50 μg/ml streptomycin (AppliChem), and 50 U/ml penicillin (AppliChem).

Pemphigus sera and IgG purification

Sera of patients with clinically confirmed PV were obtained with written and informed consent under the ethical approval of the Philipps-University of Marburg (PV1-IgG, Az20/14) or the University of Kurume (PV2-IgG, number 127). Titres of anti-DSG1 and anti-DSG3 antibodies can be found in Supplementary Table S1. Purification of IgG fractions was performed using protein A agarose as described before (Waschke et al, 2005).

Immunostaining and STED

Immunostainings were performed using standard protocols (Sigmund et al, 2023). HaCaT cells and murine KCs were fixed using 100% ethanol (at −20 °C) for 30 minutes and subsequently 100% acetone (at −20 °C) for 3 minutes or with 2% paraformaldehyde for 10 minutes and permeabilized with 0.1% Triton X-100 for 5 minutes at room temperature. Images were taken using a Leica SP5 confocal microscope with a ×63 oil-objective controlled by LAS AF software (Leica).

For STED microscopy, murine KCs were fixed with ethanol−aceton and stained as described in detail previously (Fuchs et al, 2019). Stainings were evaluated on an Abberior STED-Expert line microscope (Abberior) with IMMOIL-F30CC (Olympus GmbH) using a ×100 1.4 UPlanSApo oil-objective (Olympus).

For extended information on quantification of fluorescence staining, please refer to Supplementary Materials and Methods.

AFM

For details on experimental setup, please refer to Supplementary Materials and Methods.

For AFM experiments, we used either a setup of NanoWizard 3 AFM (JPK Instruments) mounted on an inverted optical microscope (Carl Zeiss) or NanoWizard IV AFM (JPK Instruments) mounted on an inverted microscope (IX83, Olympus). A flexible heterobifunctional benzaldehyde polyethylene glycol linker (BroadPharm) was used in accordance with previously described protocol (Ebner et al, 2007) to attach Fc-fragments containing the whole ECD of DSG1, DSG3, or DSC3, respectively, to MLCT cantilevers (Bruker). AFM data were acquired using quantitative imaging mode for topography overview images or force mapping mode for single-molecule interaction studies. Data analysis was performed using JPKSPM Data Processing software (version 6, JPK Instruments).

KC dissociation assay

KC dissociation assays were performed as described elsewhere in detail (Hartlieb et al, 2014; Walter et al, 2017). Briefly, monolayers were detached from well bottom using a mixture of Dispase II (Sigma-Aldrich) and 1% collagenase I (Thermo Fisher Scientific), and subsequently, a defined shear stress was applied by pipetting it with an electrical pipette (Eppendorf). Resulting number of fragments are an inverse measure for intercellular adhesion.

For hyper-adhesion KC dissociation assay, a well-established protocol was used (Keil et al, 2016). The Ca^{2+} chelator EGTA (5 mM) was applied for 90 minutes at 37 °C and 5% carbon dioxide on dispase/collagenase-detached monolayers in culture medium before application of a defined shear stress to test Ca^{2+} dependency.

For quantification, resulting fragments were photographed using a binocular microscope (Leica), and pictures were analyzed with ImageJ (National Institutes of Health).

Data analysis and Statistics

Figures and images were arranged and labeled using Photoshop Illustrator (Adobe). Statistical analysis was performed by Prism 8 (GraphPad Software). The cartoons were created using BioRender. AFM-unbinding force analysis was made with Origin Pro 2016, 93G (OriginLab). For multiple comparisons, we either used a 1-way or 2-way ANOVA corrected by respective Posthoc test as indicated in the respective figure legend. For comparison of 2 datasets, a 2-tailed paired Student's *t*-test was used to assign significance. We

determined a significance threshold of $*P < .05$, with error bars representing SEM. To quantify extradesmosomal vesicles, we set controls to 1; for all other quantifications, we used the mean of the respective controls.

DATA AVAILABILITY STATEMENT

All data of this study are included in the article/supplementary materials or can be requested from the corresponding author. No large datasets were generated or analyzed in this study.

ORCIDs

Letyfee Steinert: http://orcid.org/0000-0002-3244-4613
Michael Fuchs: http://orcid.org/0000-0002-7816-3438
Anna M. Sigmund: http://orcid.org/0000-0001-8533-9617
Dario Didona: http://orcid.org/0000-0002-6119-1870
Christoph Hudemann: http://orcid.org/0000-0001-5807-6882
Christian Möbs: http://orcid.org/0000-0002-5197-7669
Michael Hertl: http://orcid.org/0000-0002-5494-2461
Takashi Hashimoto: http://orcid.org/0000-0002-0144-3255
Jens Waschke: http://orcid.org/0000-0003-1182-5422
Franziska Vielmuth: https://orcid.org/0000-0002-8570-7595

CONFLICT OF INTEREST

The authors state no conflict of interest.

ACKNOWLEDGMENT

We thank Nadine Albrecht, Martina Hitzenbichler, Sabine Mühlsimer, Sabine Miech, Matthias Röhr, and Silke Gotschy for excellent technical assistance. We thank Mechthild Hatzfeld and Thomas Magin for providing cells and antibodies. This work was supported by Deutsche Forschungsgemeinschaft FOR 2497 to FV and JW.

AUTHOR CONTRIBUTIONS

Conceptualization: FV; Formal Analysis: LS, MF, FV; Funding Acquisition: FV, JW; Investigation: LS, FV, MF, AMS; Methodology: FV, LS, MF, AMS, JW; Project Administration: FV, JW; Resources: DD, CM, CH, MH, TH; Supervision: FV, JW, AMS; Validation: FV, JW; Visualization: LS, FV; Writing - Original Draft Preparation: LS, FV; Writing - Review and Editing: FV, JW, TH, LS, MF, AMS, DD, CM, CH, MH

SUPPLEMENTARY MATERIAL

Supplementary material is linked to the online version of the paper at www.jidonline.org, and at https://doi.org/10.1016/j.jid.2024.03.042.

REFERENCES

Aksu D, Peksari Y, Arica IE, Gurgey E. Assessing the autoantibody levels in relation to disease severity and therapy response in pemphigus patients. Indian J Dermatol 2010;55:342–7.

Amagai M, Karpati S, Prussick R, Klaus-Kovtun V, Stanley JR. Autoantibodies against the amino-terminal cadherin-like binding domain of pemphigus vulgaris antigen are pathogenic. J Clin Invest 1992;90:919–26.

Aoyama Y, Kitajima Y. Pemphigus vulgaris-IgG causes a rapid depletion of desmoglein 3 (Dsg3) from the Triton X-100 soluble pools, leading to the formation of Dsg3-depleted desmosomes in a human squamous carcinoma cell line, DJM-1 cells. J Invest Dermatol 1999;112:67–71.

Bartle EI, Rao TC, Beggs RR, Dean WF, Urner TM, Kowalczyk AP, et al. Protein exchange is reduced in calcium-independent epithelial junctions. J Cell Biol 2020;219:e201906153.

Bartle EI, Urner TM, Raju SS, Mattheyses AL. Desmoglein 3 order and dynamics in desmosomes determined by fluorescence polarization microscopy. Biophys J 2017;113:2519–29.

Beggs RR, Rao TC, Dean WF, Kowalczyk AP, Mattheyses AL. Desmosomes undergo dynamic architectural changes during assembly and maturation. Tissue Barriers 2022;10:2017225.

Berika M, Garrod D. Desmosomal adhesion in vivo. Cell Commun Adhes 2014;21:65–75.

Berkowitz P, Hu P, Liu Z, Diaz LA, Enghild JJ, Chua MP, et al. Desmosome signaling. Inhibition of p38MAPK prevents pemphigus vulgaris IgG-induced cytoskeleton reorganization. J Biol Chem 2005;280:23778–84.

Cheng X, Koch PJ. In vivo function of desmosomes. J Dermatol 2004;31:171–87.

Cirillo N, Lanza A, Prime SS. Induction of hyper-adhesion attenuates autoimmune-induced keratinocyte cell-cell detachment and processing of adhesion molecules via mechanisms that involve PKC. Exp Cell Res 2010;316:580–92.

Dworschak J, Recke A, Freitag M, Ludwig RJ, Langenhan J, Kreuzer OJ, et al. Mapping of B cell epitopes on desmoglein 3 in pemphigus vulgaris patients by the use of overlapping peptides. J Dermatol Sci 2012;65:102–9.

Ebner A, Wildling L, Kamruzzahan AS, Rankl C, Wruss J, Hahn CD, et al. A new, simple method for linking of antibodies to atomic force microscopy tips. Bioconjug Chem 2007;18:1176–84.

Fuchs M, Foresti M, Radeva MY, Kugelmann D, Keil R, Hatzfeld M, et al. Plakophilin 1 but not plakophilin 3 regulates desmoglein clustering. Cell Mol Life Sci 2019;76:3465–76.

Fuchs M, Kugelmann D, Schlegel N, Vielmuth F, Waschke J. Desmoglein 2 can undergo $Ca2^{+-}$dependent interactions with both desmosomal and classical cadherins including E-cadherin and N-cadherin. Biophys J 2022;121:1322–35.

Fuchs M, Radeva MY, Spindler V, Vielmuth F, Kugelmann D, Waschke J. Cytoskeletal anchorage of different Dsg3 pools revealed by combination of hybrid STED/SMFS-AFM. Cell Mol Life Sci 2023;80:25.

Fuchs M, Sigmund AM, Waschke J, Vielmuth F. Desmosomal hyperadhesion is accompanied with enhanced binding strength of desmoglein 3 molecules. Biophys J 2020;119:1489–500.

Fülle JB, Huppert H, Liebl D, Liu J, Alves de Almeida R, Yanes B, et al. Desmosome dualism - most of the junction is stable, but a plakophilin moiety is persistently dynamic. J Cell Sci 2021;134:jcs258906.

Garrod D, Chidgey M. Desmosome structure, composition and function. Biochim Biophys Acta 2008;1778:572–87.

Garrod DR. The assay that defines desmosome hyper-adhesion. J Invest Dermatol 2013;133:576–7.

Garrod DR, Berika MY, Bardsley WF, Holmes D, Tabernero L. Hyper-adhesion in desmosomes: its regulation in wound healing and possible relationship to cadherin crystal structure. J Cell Sci 2005;118:5743–54.

Getsios S, Huen AC, Green KJ. Working out the strength and flexibility of desmosomes. Nat Rev Mol Cell Biol 2004;5:271–81.

Green KJ, Simpson CL. Desmosomes: new perspectives on a classic. J Invest Dermatol 2007;127:2499–515.

Harrison OJ, Brasch J, Lasso G, Katsamba PS, Ahlsen G, Honig B, et al. Structural basis of adhesive binding by desmocollins and desmogleins. Proc Natl Acad Sci U S A 2016;113:7160–5.

Hartlieb E, Rötzer V, Radeva M, Spindler V, Waschke J. Desmoglein 2 compensates for desmoglein 3 but does not control cell adhesion via regulation of p38 mitogen-activated protein kinase in keratinocytes. J Biol Chem 2014;289:17043–53.

Hatzfeld M, Haffner C, Schulze K, Vinzens U. The function of plakophilin 1 in desmosome assembly and actin filament organization. J Cell Biol 2000;149:209–22.

Hegazy M, Perl AL, Svoboda SA, Green KJ. Desmosomal cadherins in health and disease. Annu Rev Pathol 2022;17:47–72.

Heupel WM, Zillikens D, Drenckhahn D, Waschke J. Pemphigus vulgaris IgG directly inhibit desmoglein 3-mediated transinteraction. J Immunol 2008;181:1825–34.

Hiermaier M, Kugelmann D, Radeva MY, Didona D, Ghoreschi K, Farzan S, et al. Pemphigus foliaceus autoantibodies induce redistribution primarily of extradesmosomal desmoglein 1 in the cell membrane. Front Immunol 2022;13:882116.

Hudemann C, Exner Y, Pollmann R, Schneider K, Zakrzewicz A, Feldhoff S, et al. IgG against the membrane-proximal portion of the desmoglein 3 ectodomain induces loss of keratinocyte adhesion, a hallmark in pemphigus vulgaris. J Invest Dermatol 2023;143:254–63.e3.

Ishii K, Yoshida K, Stanley JR, Yamagami J, Amagai M, Ishiko A. Pemphigus vulgaris and foliaceus IgG autoantibodies directly block heterophilic transinteraction between desmoglein and desmocollin. J Invest Dermatol 2020;140:1919–26.e7.

Kasperkiewicz M, Ellebrecht CT, Takahashi H, Yamagami J, Zillikens D, Payne AS, et al. Pemphigus. Nat Rev Dis Primers 2017;3:17026.

Keil R, Rietscher K, Hatzfeld M. Antagonistic regulation of intercellular cohesion by Plakophilins 1 and 3. J Invest Dermatol 2016;136:2022–9.

Kimura TE, Merritt AJ, Garrod DR. Calcium-independent desmosomes of keratinocytes are hyper-adhesive. J Invest Dermatol 2007;127:775–81.

Koch PJ, Mahoney MG, Ishikawa H, Pulkkinen L, Uitto J, Shultz L, et al. Targeted disruption of the pemphigus vulgaris antigen (desmoglein 3) gene in mice causes loss of keratinocyte cell adhesion with a phenotype similar to pemphigus vulgaris. J Cell Biol 1997;137:1091–102.

Lowndes M, Rakshit S, Shafraz O, Borghi N, Harmon RM, Green KJ, et al. Different roles of cadherins in the assembly and structural integrity of the desmosome complex. J Cell Sci 2014;127:2339–50.

Mao X, Nagler AR, Farber SA, Choi EJ, Jackson LH, Leiferman KM, et al. Autoimmunity to desmocollin 3 in pemphigus vulgaris. Am J Pathol 2010;177:2724–30.

Müller R, Svoboda V, Wenzel E, Gebert S, Hunzelmann N, Müller HH, et al. IgG reactivity against non-conformational NH-terminal epitopes of the desmoglein 3 ectodomain relates to clinical activity and phenotype of pemphigus vulgaris. Exp Dermatol 2006;15:606–14.

Müller R, Svoboda V, Wenzel E, Müller HH, Hertl M. IgG against extracellular subdomains of desmoglein 3 relates to clinical phenotype of pemphigus vulgaris. Exp Dermatol 2008;17:35–43.

Oktarina DA, van der Wier G, Diercks GF, Jonkman MF, Pas HH. IgG-induced clustering of desmogleins 1 and 3 in skin of patients with pemphigus fits with the desmoglein nonassembly depletion hypothesis. Br J Dermatol 2011;165:552–62.

Owen GR, Stokes DL. Exploring the nature of desmosomal cadherin associations in 3D. Dermatol Res Pract 2010;2010:930401.

Price AJ, Cost AL, Ungewiss H, Waschke J, Dunn AR, Grashoff C. Mechanical loading of desmosomes depends on the magnitude and orientation of external stress. Nat Commun 2018;9:5284.

Rafei D, Müller R, Ishii N, Llamazares M, Hashimoto T, Hertl M, et al. IgG autoantibodies against desmocollin 3 in pemphigus sera induce loss of keratinocyte adhesion. Am J Pathol 2011;178:718–23.

Schlögl E, Radeva MY, Vielmuth F, Schinner C, Waschke J, Spindler V. Keratin retraction and desmoglein3 internalization independently contribute to autoantibody-induced cell dissociation in pemphigus vulgaris. Front Immunol 2018;9:858.

Schmidt E, Kasperkiewicz M, Joly P. Pemphigus. Lancet 2019;394:882–94.

Schmitt T, Hudemann C, Moztarzadeh S, Hertl M, Tikkanen R, Waschke J. Dsg3 epitope-specific signalling in pemphigus. Front Immunol 2023;14:1163066.

Sekiguchi M, Futei Y, Fujii Y, Iwasaki T, Nishikawa T, Amagai M. Dominant autoimmune epitopes recognized by pemphigus antibodies map to the N-terminal adhesive region of desmogleins. J Immunol 2001;167:5439–48.

Shafraz O, Rübsam M, Stahley SN, Caldara AL, Kowalczyk AP, Niessen CM, et al. E-cadherin binds to desmoglein to facilitate desmosome assembly. eLife 2018;7:e37629.

Sigmund AM, Steinert LS, Egu DT, Bayerbach FC, Waschke J, Vielmuth F. Dsg2 upregulation as a rescue mechanism in pemphigus. Front Immunol 2020;11:581370.

Sigmund AM, Winkler M, Engelmayer S, Kugelmann D, Egu DT, Steinert LS, et al. Apremilast prevents blistering in human epidermis and stabilizes keratinocyte adhesion in pemphigus. Nat Commun 2023;14:116.

Spindler V, Eming R, Schmidt E, Amagai M, Grando S, Jonkman MF, et al. Mechanisms causing loss of keratinocyte cohesion in pemphigus. J Invest Dermatol 2018;138:32–7.

Spindler V, Heupel WM, Efthymiadis A, Schmidt E, Eming R, Rankl C, et al. Desmocollin 3-mediated binding is crucial for keratinocyte cohesion and is impaired in pemphigus. J Biol Chem 2009;284:30556–64.

Spindler V, Waschke J. Desmosomal cadherins and signaling: lessons from autoimmune disease. Cell Commun Adhes 2014;21:77–84.

Spindler V, Waschke J. Pemphigus-a disease of desmosome dysfunction caused by multiple mechanisms. Front Immunol 2018;9:136.

Tsunoda K, Ota T, Aoki M, Yamada T, Nagai T, Nakagawa T, et al. Induction of pemphigus phenotype by a mouse monoclonal antibody against the amino-terminal adhesive interface of desmoglein 3. J Immunol 2003;170:2170–8.

Tucker DK, Stahley SN, Kowalczyk AP. Plakophilin-1 protects keratinocytes from pemphigus vulgaris IgG by forming calcium-independent desmosomes. J Invest Dermatol 2014;134:1033–43.

Ungewiss H, Rötzer V, Meir M, Fey C, Diefenbacher M, Schlegel N, et al. Dsg2 via Src-mediated transactivation shapes EGFR signaling towards cell adhesion [published correction appears in Cell Mol Life Sci 2019;76:3477]. Cell Mol Life Sci 2018;75:4251–68.

Vielmuth F, Spindler V, Waschke J. Atomic force microscopy provides new mechanistic insights into the pathogenesis of pemphigus. Front Immunol 2018a;9:485.

Vielmuth F, Walter E, Fuchs M, Radeva MY, Buechau F, Magin TM, et al. Keratins regulate p38MAPK-dependent desmoglein binding properties in pemphigus. Front Immunol 2018b;9:528.

Vielmuth F, Wanuske MT, Radeva MY, Hiermaier M, Kugelmann D, Walter E, et al. Keratins regulate the adhesive properties of desmosomal cadherins through signaling. J Invest Dermatol 2018c;138:121–31.

Vielmuth F, Waschke J, Spindler V. Loss of desmoglein binding is not sufficient for keratinocyte dissociation in pemphigus. J Invest Dermatol 2015;135:3068–77.

Walter E, Vielmuth F, Rotkopf L, Sárdy M, Horváth ON, Goebeler M, et al. Different signaling patterns contribute to loss of keratinocyte cohesion dependent on autoantibody profile in pemphigus. Sci Rep 2017;7:3579.

Waschke J. The desmosome and pemphigus. Histochem Cell Biol 2008;130:21–54.

Waschke J, Bruggeman P, Baumgartner W, Zillikens D, Drenckhahn D. Pemphigus foliaceus IgG causes dissociation of desmoglein 1-containing junctions without blocking desmoglein 1 transinteraction. J Clin Invest 2005;115:3157–65.

Waschke J, Spindler V. Desmosomes and extradesmosomal adhesive signaling contacts in pemphigus. Med Res Rev 2014;34:1127–45.

Weiss D, Ristl R, Griss J, Bangert C, Foedinger D, Stingl G, et al. Autoantibody levels and clinical disease severity in patients with pemphigus: comparison of aggregated anti-desmoglein ELISA values and indirect immunofluorescence titres. Acta Derm Venereol 2015;95:559–64.

Wilgram GF, Caulfield JB, Lever WF. An electron microscopic study of acantholysis in pemphigus vulgaris. J Invest Dermatol 1961;36:373–82.

SUPPLEMENTARY MATERIALS AND METHODS

Cell culture

Wild-type murine epidermal keratinocytes (KCs) are a kind gift of Mechthild Hatzfeld (Division of Pathobiochemistry, Institute of Molecular Medicine, Martin-Luther-University Halle-Wittenberg, Halle, Germany). Murine KCs were cultivated in low-calcium complete FAD media (0.05 mM calcium chloride, PAN Biotech) on collagen I (rat tail, BD Bioscience) as previously described (Fuchs et al, 2020; Sigmund et al, 2020). To induce differentiation, confluent murine KCs were switched to high-calcium–containing medium (1.2 mM) and were cultivated therein for 24–36 hours for nonhyperadhesive or 96 hours for hyperadhesive experiments. HaCaT cells are a kind gift from Petra Boukamp (German Cancer Research Center, Heidelberg, Germany) and cultivated in DMEM (Life Technologies) containing 1.8 mM calcium supplemented with 10% fetal bovine serum (Sigma-Aldrich), 50 μg/ml streptomycin (AppliChem), and 50 U/ml penicillin (AppliChem). All cells were grown at 37 °C in a 5% carbon dioxide atmosphere. The nonhyperadhesive time point was determined on the basis of hyperadhesion dissociation assays. Atomic force microscopy (AFM) experiments in which the cells were treated for 1 hour had a differentiation time in high-calcium medium for 24 hours. In all other experiments in which the cells were treated 24 hours before the experiment, we chose a differentiation period in high-calcium medium of 36 hours. The differentiation time for hyperadhesive cells was 96 hours for all experiments. The effective dose of pemphigus vulgaris IgG, AK23, 2G4, or anti-DSC3 was determined in previous studies (Hudemann et al, 2023; Spindler et al, 2009; Vielmuth et al, 2015) and validated by an equal dose of control IgG.

Immunostaining and stimulated emission depletion microscopy

Immunostainings were performed using standard protocols. HaCaT cells and murine KCs were grown on 12-mm glass coverslips (VWR International). Murine KCs were fixed using 100% ethanol (at −20 °C) for 30 minutes and subsequently with 100% aceton (at −20 °C) for 3 minutes. HaCaT cells were fixed with 2% paraformaldehyde for 10 minutes and permeabilized with 0.1 % Triton X-100 for 5 minutes at room temperature. Subsequently, both samples were treated with 3% BSA and 1% normal goat serum for 20 minutes at room temperature to block unspecific antibody binding. Murine KCs were incubated with desmoglein (DSG) 3 (number ELA-E-AB-62720-120, Biozol/Elabsicience) and DSG1 (Santa Cruz Biotechnology, number sc-137164). For cytokeratin staining, we incubated the cells with cytokeratin 14 (abcam, ab7800) and cytokeratin 5 (kind gift of Thomas Magin group). Cy3-conjugated goat anti-mouse/rabbit and Cy2-conjugated goat anti-rabbit/mouse antibodies (Dianova) were applied for 1 hour, and DAPI (number D9542, Sigma-Aldrich) at 1:10,000 was incubated for 10 minutes at room temperature. The samples were mounted in neopentyl glycol (number P3130, Sigma-Aldrich), and images were taken using a Leica SP5 confocal microscope with a ×63 oil-objective controlled by LAS AF software (Leica). For immunofluorescence quantification, the fluorescence intensity was measured at small areas at the cell border and analyzed with ImageJ (National Institutes of Health).

For stimulated emission depletion microscopy, murine KCs were seeded on #1.5 coverslips (VWR International) and fixed with ethanol–aceton as described earlier. They were coimmunostained with the following couples: DSG1 (number sc-137164, Santa Cruz Biotechnology) and desmoplakin (Dp) (number A7635, Abclonal), DSG3 (number ELA-E-AB-62720-120, Biozol/Elabsicience) and Dp1+2 (number 61003, Progen), and DSC3 (clone U114, number 65193, Progen) and Dp (number A7635, Abclonal). As second antibodies, STAR-RED–coupled (number 2-0002-011-2, Abberior) or Alexa 594–coupled (number A-11014, Thermo Fisher Scientific) goat anti-rabbit/mouse secondary antibodies were incubated for 1 hour, and DAPI at 1:10,000 was applied for 10 minutes at room temperature. The stained samples were mounted in Prolong Diamond Antifade (number P36961, Thermo Fisher Scientific) and evaluated on an Abberior STED Expert line microscope (Abberior) with IMMOIL-F30CC (Olympus GmbH) using a ×100 1.4 UPlanSApo oil-objective (Olympus).

To quantify extradesmosomal cadherins, the width of the Dp plaques was measured. They had an average of 0.36 μm in nonhyperadhesive and 0.66 μm in hyperadhesive KCs to define the plasma membrane proximal area. Subsequently, a line with this respective width was drawn along the cell membranes to define DSG3 molecules localized to the cell membrane. A threshold was determined with images from second antibody control stainings, and pixels below this threshold were excluded from analysis. Next, all molecules that were colocalized to Dp were excluded, and the remaining DSG3-positive pixels were defined as extradesmosomal and analyzed with regard to intensity. The fluorescence intensity/area was calculated and compared between control and antibody condition, showing a significant reduction under incubation with the respective antibodies. For each experiments, the average of >3 independent cell borders was used.

Colocalization of Dp and the respective desmosomal cadherin was identified by the ImageJ plugin (https://imagej.net/ij/plugins/colocalization-finder.html), which provides a pixel-wise quantification method on the basis of a scatter plot technique, whereby a threshold was applied to exclude background staining. The background was defined in the images obtained from the second antibody control experiment. Percentage of colocalized pixels refers to all pixels that were above the threshold in both stainings in relation to all pixels of the given image. The desmosomal length was calculated at a defined length of 5 μm, including 3 different membranes in each n.

Purification of recombinant DSG/DSC-Fc constructs

DSG- and DSC-Fc constructs for AFM measurements were purified as described before (Heupel et al, 2008). DSG1, DSG3, and DSC3-Fc constructs, containing the entire extracellular domain of the respective protein, were expressed in Chinese hamster ovarian cells. After the cells reach confluence, the supernatant was collected and purified with protein-A agarose affinity purification chromatography (Life Technologies). Finally, the purification was validated by a western blot with the respective anti-DSG1 (p124, Progen), anti-DSG3

(clone 5G11, Life Technologies), anti-DSC3 (clone U114, number 65193, Progen), or anti-DSG2 (BM5016, OriGene Technologies) mAb and a Coomassie staining.

AFM

Live-cell interaction studies were performed with both adhesive states of murine KCs and HaCaT cells. For AFM analysis, 50 × 50 μm overview quantitative images were taken to investigate the cell topography. Subsequently, single-molecule interactions were measured using the force mapping mode. To determine the single-molecule adhesion properties, including binding frequency and unbinding force, 4 × 2 μm rectangles of the cell border or cell surface nuclear area were selected, and force–distance curves were recorded in a pixel-wise manner.

For AFM measurements, MLCT cantilevers with a spring constant of 0.03 N/m, a tip radius of 20 nm, and pyramidal-shaped D-Tips of Si3N4 (Bruker, Mannheim, Germany) were used for adhesion measurements; the tip of the cantilever was linked with Fc-fragments of the respective desmosomal cadherin protein (0.15 mg/ml) through a flexible heterobifunctional benzaldehyde polyethylene glycol linker (Broadpharm) as described before in detail (Ebner et al, 2007). The tip–surface interaction was 0.1 s with an indentation force of 0.5 nN and a retraction of 2 μm with 10 μm/s. After 2 control measurements on 2 distinct cell borders, cells were incubated with pemphigus vulgaris IgG for 1 hour, whereas the scanning tip was removed to avoid antibody binding to the scanning tip. After treatment, the cells were washed 3 times with 1× PBS to remove unbound antibodies, and the KCs were measured again. Both adhesive conditions were analyzed with the same coated cantilever scanning tip. To determine the unbinding force, acquired binding events per n were analyzed using a multiple Extreme fit.

To investigate the effect of direct inhibition of pathogenic pemphigus antibodies on desmosomal cadherin interactions in both adhesive states, we used the following antibodies: DSC3 (clone U114, 1:50 dilution, number 65193, Progen, targets extracellular domain 5), AK23 (75 μg/ml, targets extracellular domain 1), 2G4 (75 μg/ml, targets extracellular domain 5), PV1-IgG (dilution 1:50, polyclonal), PV2-IgG (dilution 1:50, polyclonal), DSG2 (BM5016, OriGene Technologies), and DSG3 (clone5G11, Life Technologies). The specific binding domain of the respective antibody is shown in Supplementary Figure S4c.

SUPPLEMENTARY REFERENCES

Ebner A, Wildling L, Kamruzzahan AS, Rankl C, Wruss J, Hahn CD, et al. A new, simple method for linking of antibodies to atomic force microscopy tips. Bioconjug Chem 2007;18:1176–84.

Fuchs M, Sigmund AM, Waschke J, Vielmuth F. Desmosomal hyperadhesion is accompanied with enhanced binding strength of desmoglein 3 molecules. Biophys J 2020;119:1489–500.

Heupel WM, Zillikens D, Drenckhahn D, Waschke J. Pemphigus vulgaris IgG directly inhibit desmoglein 3-mediated transinteraction. J Immunol 2008;181:1825–34.

Hudemann C, Exner Y, Pollmann R, Schneider K, Zakrzewicz A, Feldhoff S, et al. IgG against the membrane-proximal portion of the desmoglein 3 ectodomain induces loss of keratinocyte adhesion, a hallmark in pemphigus vulgaris. J Invest Dermatol 2023;143:254–63.e3.

Sigmund AM, Steinert LS, Egu DT, Bayerbach FC, Waschke J, Vielmuth F. Dsg2 upregulation as a rescue mechanism in pemphigus. Front Immunol 2020;11:581370.

Spindler V, Heupel WM, Efthymiadis A, Schmidt E, Eming R, Rankl C, et al. Desmocollin 3-mediated binding is crucial for keratinocyte cohesion and is impaired in pemphigus. J Biol Chem 2009;284:30556–64.

Vielmuth F, Hartlieb E, Kugelmann D, Waschke J, Spindler V. Atomic force microscopy identifies regions of distinct desmoglein 3 adhesive properties on living keratinocytes. Nanomedicine 2015;11:511–20.

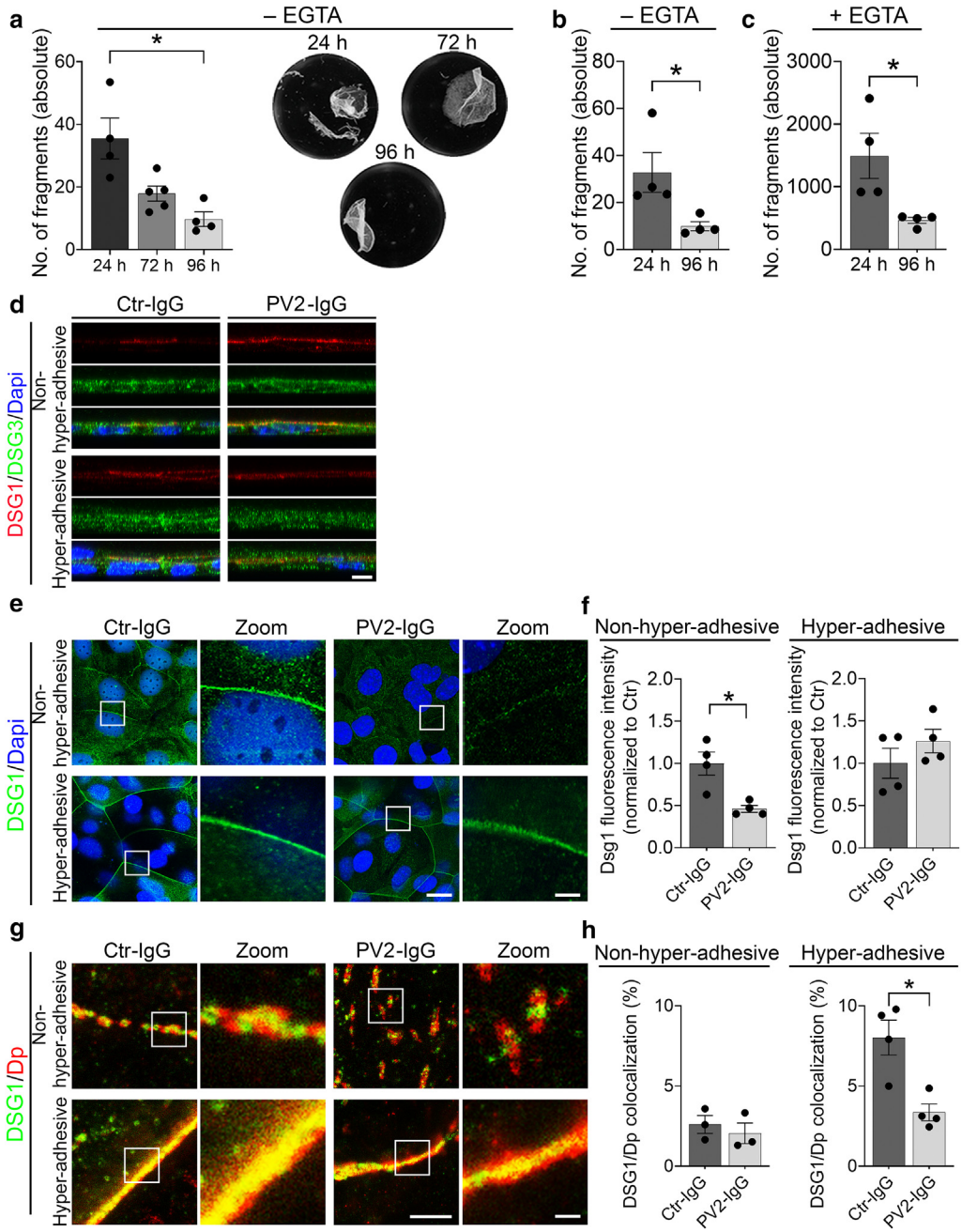

Supplementary Figure S1. PV2-IgG–induced DSG1 depletion is diminished in hyper-adhesive WT murine KCs. (**a**) Dissociation assay in murine KCs showed that fragmentation of the cell monolayer decreased over time up to 96 h. Longer differentiation time increased fragmentation again owing to dying of the cells (n $\geq$ 4, means ± SEM, *$P < .05$; 1-way ANOVA with Bonferroni correction). (**b**) Dissociation assay (−EGTA) and (**c**) hyper-adhesion dissociation assay (+EGTA) in HaCaT cells revealed that KCs become hyper-adhesive after 96 h in high-Ca^{2+} medium because fragmentation was significantly reduced (n $\geq$ 4, means ± SEM, *$P < .05$). (**d**) Immunostaining of DSG1 and DSG3 after incubation with PV2-IgG for 1 h showed an unchanged membrane intensity and localization of both in non-hyper-adhesive and hyper-adhesive murine KCs. Bar = 10 μm (representative n = 4). (**e**) Immunostaining of murine KCs revealed a strong loss of DSG1 and membrane fragmentation after PV2-IgG, which was diminished but not absent in hyper-adhesive KCs (representative n $\geq$ 4). Bar = 20 μm; zoom = 5 μm. (**f**) Quantification of DSG1 cell membrane intensity indicated a reduction of DSG1 after incubation with PV2-IgG for 24 h only in non-hyper-adhesive cells (n = 4, means normalized to Ctr ± SEM, *$P < .05$). (**g**) DSG1/Dp costaining in STED analysis confirmed PV2-IgG–induced fragmentation of DSG1 membrane staining in non-hyper-adhesive cells and delineates the reduction of extradesmosomal membrane-proximal DSG1 vesicle in both adhesion states after treatment with PV2-IgG (representative n = 4). Bar = 5 μm; zoom = 1 μm. (**h**) DSG1/Dp colocalization was slightly reduced in non-hyper-adhesive KCs and was still compromised in hyper-adhesive murine KCs (n $\geq$ 3, means ± SEM, *$P < .05$). Ca^{2+}, calcium ion; Ctr, control; Dp, desmoplakin; DSG, desmoglein; h, hour; KC, keratinocyte; PV, pemphigus vulgaris; STED, stimulated emission depletion; WT, wild-type.

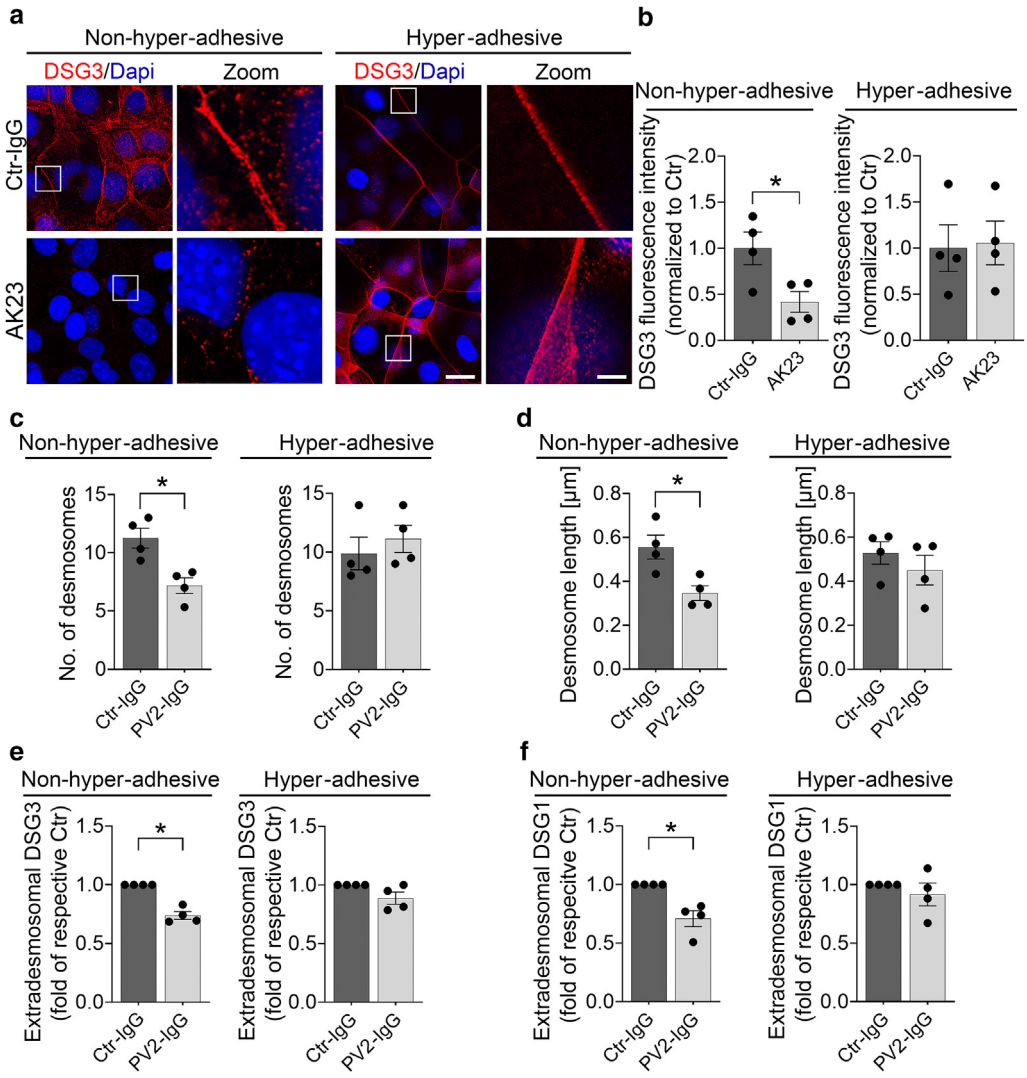

Supplementary Figure S2. Hyper-adhesiveness abolishes PV-IgG–induced DSG depletion and ameliorates changes in the number and length of desmosomes. (**a**) Immunostaining of DSG3 in non-hyper-adhesive (36 h in high-Ca^{2+} medium) and hyper-adhesive (96 h in high-Ca^{2+} medium) WT murine KC revealed a continuous membrane staining under control condition. AK23 (24 h prior to experiment) led to a fragmentation of the DSG3 membrane staining as well as reduced fluorescence intensity in non-hyper-adhesive but not in hyper-adhesive KCs (representative $n \geq 4$). Bar = 20 µm; zoom = 5 µm. (**b**) Only non-hyper-adhesive murine KCs showed a reduced DSG3 membrane staining after incubation with AK23 for 24 h ($n = 4$, means normalized to Ctr ± SEM, $^*P < .05$). In STED experiments, (**c**) overall number and (**d**) length of desmosomes, measured through STED by Dp staining, were reduced after PV-IgG treatment in non-hyper-adhesive but not in hyper-adhesive KCs ($n = 4$, means ± SEM, $^*P < .05$). (**e**) STED quantification of extradesmosomal DSG3 demonstrated that PV2-IgG (24 h prior to experiment) induced reduction of extradesmosomal DSG3 in non-hyper-adhesive but not in hyper-adhesive murine KCs ($n \leq 5$, means normalized to Ctr ± SEM, $^*P < .05$). (**f**) Same results were observed for extradesmosomal DSG1 ($n = 4$, means normalized to Ctr ± SEM, $^*P < .05$). Ca^{2+}, calcium ion; Ctr, control; Dp, desmoplakin; DSG, desmoglein; h, hour; KC, keratinocyte; PV, pemphigus vulgaris; STED, stimulated emission depletion; WT, wild-type.

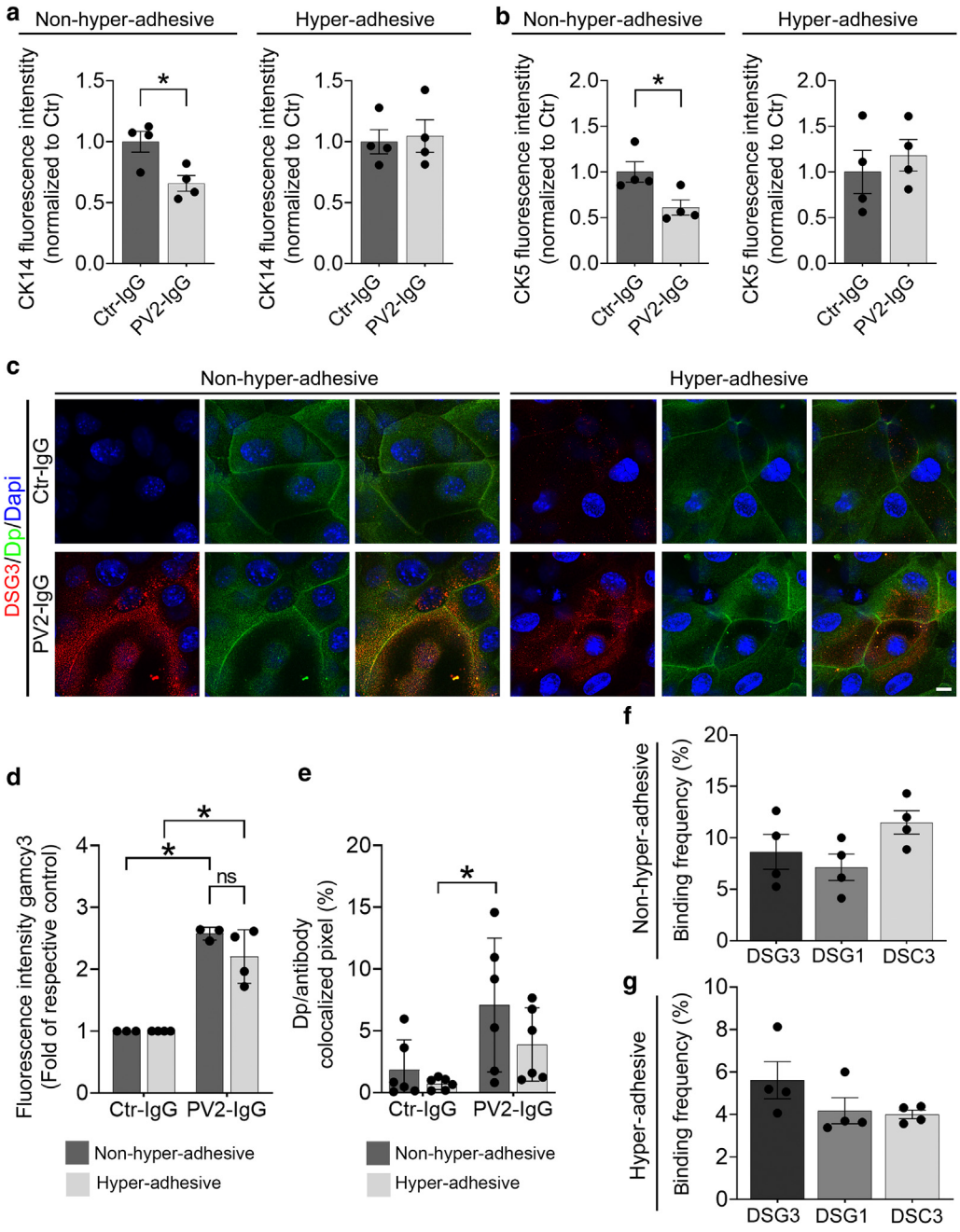

Supplementary Figure S3. PV-IgG–mediated changes in the keratin cytoskeleton are absent in hyper-adhesive KCs, and antibody binding does not differ between the distinct adhesive states. (**a**) Quantification of CK14 in the cell border area highlighted a significant reduction only in non-hyper-adhesive (36 h in high-Ca^{2+} medium) murine KCs when the cell were preincubated with PV2-IgG (24 h prior to experiment) (n = 4, means normalized to Ctr ± SEM, $*P < .05$). (**b**) The same observation was confirmed for CK5 (n = 4, means normalized to Ctr ± SEM, $*P < .05$). (**c**) Immunostaining of gah-cy3 and Dp in non-hyper-adhesive (24 h in high-Ca^{2+} medium) and hyper-adhesive (96 h in high-Ca^{2+} medium) murine KCs, previously incubated with Ctr-IgG and PV2-IgG for 1 h. Ctr-IgG was almost completely absent in both adhesive states, whereas PV2-IgG was bound in both adhesive states to the same extent. (**d**) Quantification of membrane-bound PV IgG from **c** (representative n = 4). Bar = 10 μm (n ≥ 3, means normalized to Ctr ± SEM, $*P < .05$; 2-way ANOVA with Tukey's correction). (**e**) Colocalization analysis of gah-cy3 and Dp showed no changes in binding of PV IgGs under non-hyper-adhesive and hyper-adhesive conditions (n ≥ 4, means ± SEM, $*P < .05$; 2-way ANOVA with Tukey's correction). (**f, g**) AFM adhesion measurements of DSG1-, DSG3-, and DSC3-coated cantilevers on non-hyper-adhesive and hyper-adhesive murine KCs revealed an average binding frequency of ~6–12% in non-hyper-adhesive cells and 4–6% in hyper-adhesive cells (n = 4, from 4 independent coating procedures, 2 cell border adhesion maps with 800 force–distance curves/adhesion map, means ± SEM, $*P < .05$). AFM, atomic force microscopy; Ca^{2+}, calcium ion; CK14, cytokeratin 14; CK5, cytokeratin 5; Ctr, control; Dp, desmoplakin; DSG, desmoglein; h, hour; KC, keratinocyte; ns, not significant; PV, pemphigus vulgaris.

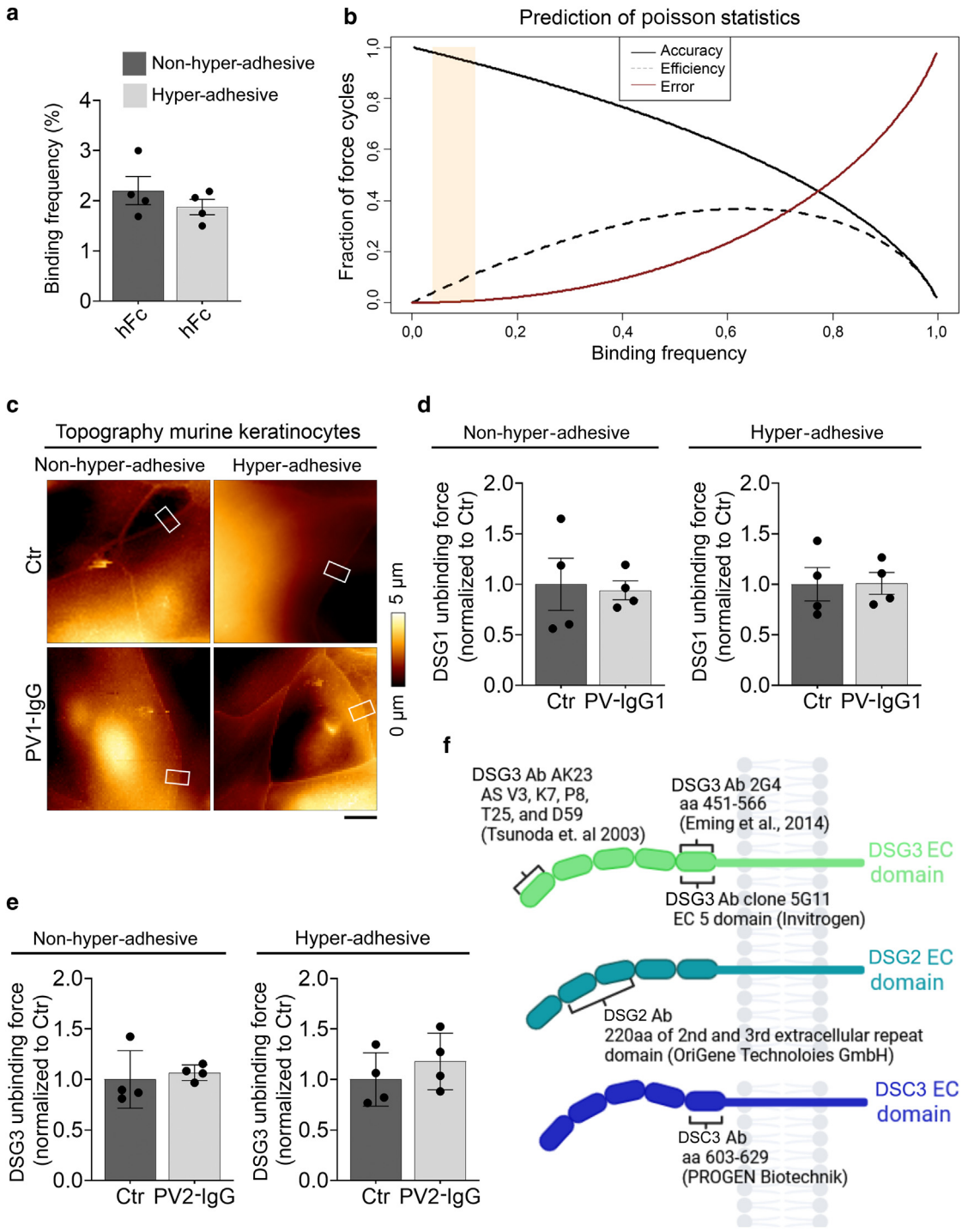

Supplementary Figure S4. The specificity of AFM single-molecule measurements is validated by interaction measurements with hFc and Poisson statistic. (**a**) AFM adhesion measurements on murine KCs in both adhesive states (24 or 96 h in high-Ca^{2+} medium) with hFc-fragment–coated cantilever showed a binding frequency of ~2%, determined as unspecific binding events (n = 4, from 4 independent coating procedures, 2 cell border adhesion maps with 800 force–distance curves/adhesion map, means ± SEM, $*P < .05$). (**b**) Poisson statistic predicted 94 and 98% probability to measure single-molecule interactions when the binding frequency is between 4 and 12%. (**c**) AFM overview topography measurements in non-hyper-adhesive (24 h in high-Ca^{2+} medium) and hyper-adhesive (96 h in high-Ca^{2+} medium) murine KCs before (Ctr) and after treatment with PV1 IgG for 1 h showed no changes in the cellular topography (representative n ≥ 4). (**d**) AFM-unbinding force measurements of DSG1 did not show any significant change of both adhesion states (24 and 96 h in high-Ca^{2+} medium) before and after treatment with PV1-IgG (n = 4, from 4 independent coating procedures, 2 cell border adhesion maps with 800 force–distance curves/adhesion map, means of extreme fits normalized to Ctr ± SEM, $*P < .05$). (**e**) In DSG3 AFM adhesion measurements, the DSG3-unbinding force was not affected by PV2-IgG application for 1 h in both adhesion states (24 or 96 h in high-Ca^{2+} medium) (n = 4, from = 4 independent coating procedures, 2 cell border adhesion maps with 800 force–distance curves/adhesion map, means of extreme fits normalized to Ctr ± SEM, $*P < .05$). (**f**) Binding epitopes of different DSG3, DSG2, and DSC3 commercially available pathogenic antibodies. aa, amino acid; Ab, antibody; AFM, atomic force microscopy; Ca^{2+}, calcium ion; Ctr, control; DSG, desmoglein; h, hour; KC, keratinocyte; PV, pemphigus vulgaris.

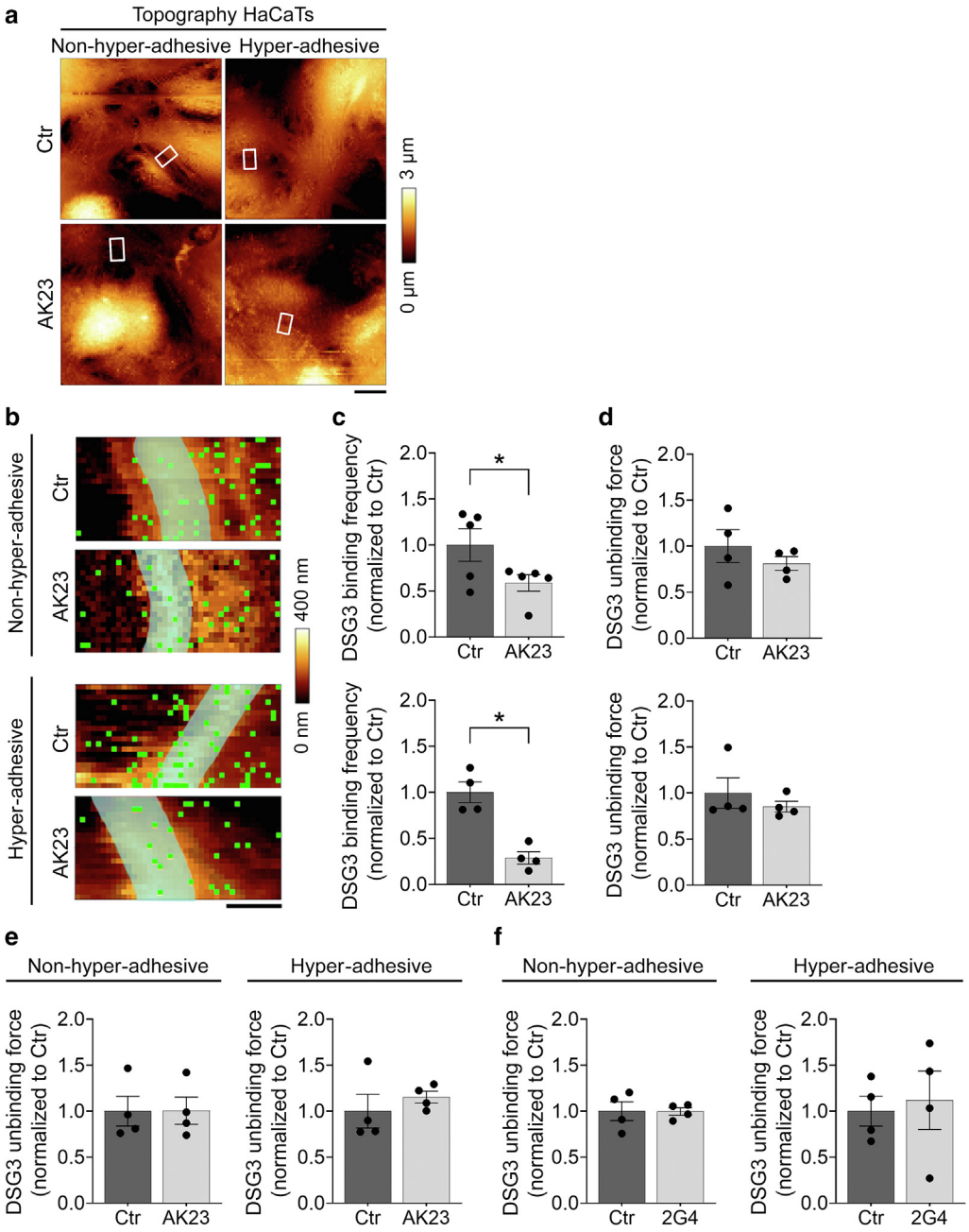

Supplementary Figure S5. DSG3 antibodies directed against several parts of the DSG3 ECD do not change DSG3-unbinding forces. (**a**) AFM overview topography measurements in non-hyper-adhesive (24 h in high-Ca^{2+} medium) and hyper-adhesive (96 h in high-Ca^{2+} medium) HaCaT cells before (Ctr) and after treatment with AK23 for 1 h induced no changes in the overall cellular topography (representative n $\geq$ 4). (**b**–**d**) Murine KCs showed AK23-induced DSG3-direct inhibition in hyper-adhesive and non-hyper-adhesive cells. (**b**) AFM adhesion maps for DSG3 across cell borders of murine KCs under non-hyper-adhesive (24 h in -highCa^{2+} medium) and hyper-adhesive (96 h in high-Ca^{2+} medium) conditions. Every green dot represents 1 DSG3-dependent binding event. AK23 incubation for 1 h led to a drastic reduction in binding frequency in both adhesive states. Bar = 1 µm. (**c**) Quantification of the binding frequency and (**d**) the unbinding force confirmed that AK23 induced a strong direct inhibition in both adhesion states but had no impact on the DSG3-specific binding strength (n $\geq$ 4, from 4 independent coating procedures, 2 cell border adhesion maps with 800 force–distance curves/adhesion map, means normalized to Ctr $\pm$ SEM, *P < .05). (**e**) Unbinding forces of DSG3-specific binding events were not changed in non-hyper-adhesive and hyper-adhesive cells after treatment with AK23 for 1 h (n = 4, from 4 independent coating procedures, 2 cell border adhesion maps with 800 force–distance curves/adhesion map, means of extreme fits normalized to Ctr $\pm$ SEM, *P < .05). (**f**) In line with previous results, we observed that the unbinding force of DSG3-specific binding events was not changed in both adhesion states (24 or 96 h in high-Ca^{2+} medium) after 2G4 incubation for 1 h (n = 4, from 4 independent coating procedures, 2 cell border adhesion maps with 800 force–distance curves/adhesion map, means of extreme fits normalized to Ctr $\pm$ SEM, *P < .05). AFM, atomic force microscopy; Ca^{2+}, calcium ion; Ctr, control; DSG, desmoglein; ECD, extracellular domain; h, hour; KC, keratinocyte.

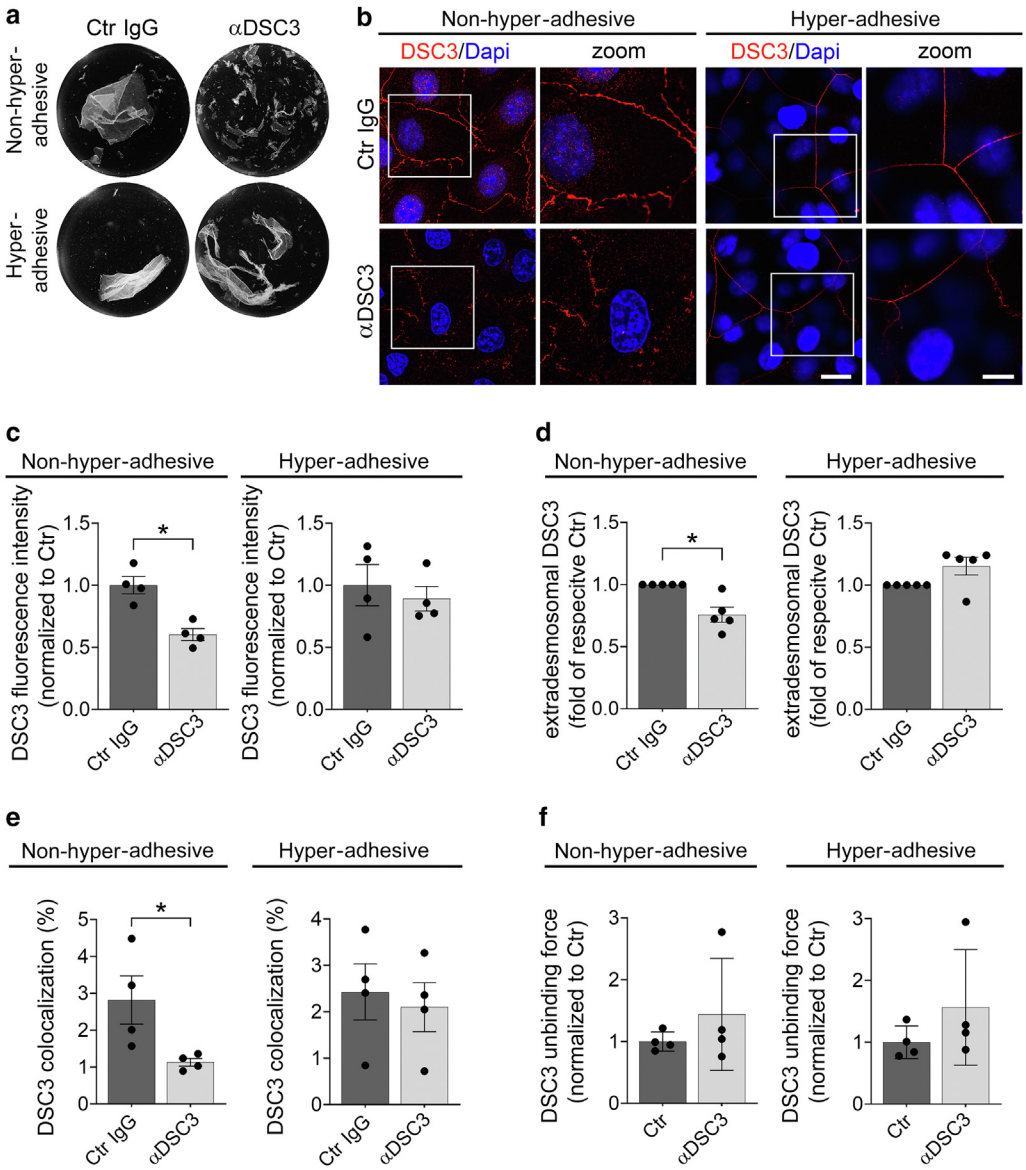

Supplementary Figure S6. A commercial anti-DSC3 antibody led to a compromised cell adhesion with reduced desmosomal and extradesmosomal DSC3 and diminished DSC3/Dp colocalization in non-hyper-adhesive KCs. (**a**) KC dissociation assay of WT KCs after treatment with Ctr-IgG or an anti-DSC3 antibody for 24 h revealed strong effect of anti-DSC3 on non-hyper-adhesive (36 h in high-Ca^{2+} medium) cells (representative n ≥ 4). (**b**) The anti-DSC3 antibody led to serration and decrease of DSC3 immunostaining intensity only in non-hyper-adhesive (36 h in high-Ca^{2+} medium) WT murine KCs, whereas hyper-adhesive cells (96 h in high-Ca^{2+} medium) showed no impairment caused by the pathogenic anti-DSC3 antibody (representative n = 4) (bar = 20 μm; zoom = 10 μm). (**c**) Quantification of fluorescence intensity of DSC3, which was significantly decreased after incubating with an anti-DSC3 antibody for 1 h in non-hyper-adhesive (36 h in high-Ca^{2+}medium) murine KCs (n = 4, means normalized to Ctr ± SEM, *$P < .05$). (**d**) STED quantification revealed a significant extradesmosomal DSC3 fluorescence intensity reduction after previous incubation with anti-DSC3 for 1 h. This effect was only detectable in non-hyper-adhesive murine KCs (n = 5, means normalized to Ctr ± SEM, *$P < .05$). (**e**) Colocalization of DSC3/Dp in non-hyper-adhesive (36 h in high-Ca^{2+}medium) cells was reduced after PV2-IgG incubation for 24 h (n = 4, means ± SEM, *$P < .05$). (**f**) In DSC3 AFM adhesion measurements, the DSC3-unbinding force was not affected by anti-DSC3 application for 1 h in both adhesion states (n = 4, from 4 independent coating procedures, 2 cell border adhesion maps with 800 force–distance curves/adhesion map, means of extreme fits normalized to Ctr ± SEM, *$P < .05$). AFM, atomic force microscopy; Ca^{2+}, calcium ion; Ctr, control; Dp, desmoplakin; h, hour; KC, keratinocyte; PV, pemphigus vulgaris; STED, stimulated emission depletion; WT, wild-type.

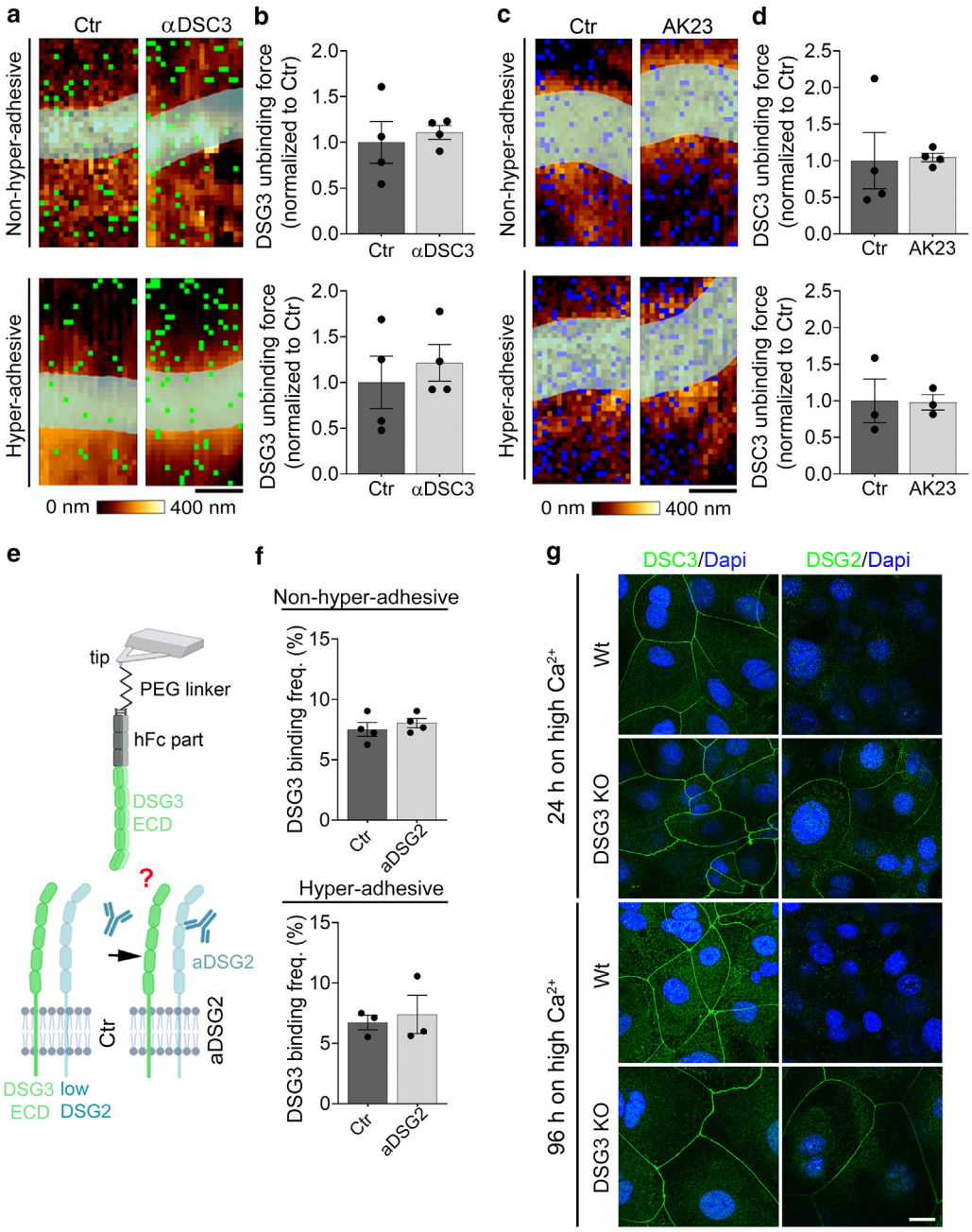

Supplementary Figure S7. Antibody experiments indicate that no DSG3−DSC3 or DSG3−DSG2 interactions are present under both adhesive states in WT KCs, whereas DSG2 is upregulated in DSG3-KO KCs. (**a**) AFM adhesion maps of murine KCs for DSG3 across cell borders of murine KCs under non-hyper-adhesive (24 h in high-Ca^{2+} medium) and hyper-adhesive (96 h in high-Ca^{2+} medium) conditions. Every green dot represents 1 DSG3-dependent binding event. Anti-DSC3 incubation for 1 h had no impact on the binding events in both states of adhesion (representative n ≥ 4). Bar = 1 μm. (**b**) AFM-unbinding force measurements of DSG3 did not show any significant change of both adhesion states before and after treatment with anti-DSC3 for 1 h (n = 4, from 4 independent coating procedures, 2 cell border adhesion maps with 800 force−distance curves/adhesion map, means of extreme fits normalized to Ctr ± SEM, $*P < .05$). (**c**) AFM adhesion maps of murine KCs for DSC3 across cell borders of murine KCs under non-hyper-adhesive (24 h in high-Ca^{2+} medium) and hyper-adhesive (96 h in high-Ca^{2+} medium) conditions. DSC3-binding events (represented by blue dots) revealed no difference of both adhesion states before and after incubation with an anti-DSC3 antibody for 1 h (representative n ≥ 4). Bar = 1 μm. (**d**) There were no changes in the DSC3-unbinding force in non-hyper-adhesive and hyper-adhesive cells after application of AK23 for 1 h (n ≥ 3, from ≥ 3 independent coating procedures, 2 cell border adhesion maps with 800 force−distance curves/adhesion map, means of extreme fits normalized to Ctr ± SEM, $*P < .05$). (**e**) Schematic of AFM measurement with DSG3-coated tip. The commercial monoclonal anti-DSG2 was binding on the DSG2 ECD2/3 and was solely incubated on the cells to avoid antibody binding to the scanning tip. (**f**) WT murine KCs were incubated with anti-DSG2 mAb, which was not able to block DSG3 interactions in WT murine KCs in both adhesive states (24 and 96 h in high-Ca^{2+} medium) (n = 4, from 4 independent coating procedures, 2 cell border adhesion maps with 800 force−distance curves/adhesion map, means ± SEM, $*P < .05$). (**g**) Immunostaining of DSC3 and DSG2 in WT and DSG3-KO murine KCs differentiated between 24 and 96 h in high-Ca^{2+} medium. DSC3 staining showed no changes in WT and DSG3-KO KCs during differentiation. DSG2 was almost absent along membranes in WT non-hyper-adhesive and hyper-adhesive cells. In contrast, in DSG3-KO murine KCs, DSG2 was upregulated along cell borders for both differentiation times (representative n = 4) (bar = 20 μm). AFM, atomic force microscopy; Ca^{2+}, calcium ion; Ctr, control; DSG, desmoglein; ECD, extracellular domain; h, hour; KC, keratinocyte; KO, knockout; PEG, polyethylene glycol; WT, wild-type.

Supplementary Figure S8. DSG3-KO KCs show heterophilic DSG2–DSG3 interactions. (**a**) Schematic of AFM measurement with DSG3-coated tip. The commercial monoclonal anti-DSG3 antibody 5G11 binds the ECD5 of DSG3 and was solely incubated on the cells to avoid antibody binding to the scanning tip. (**b**) In contrast to WT KCs, the DSG3-binding frequency of DSG3-KO KCs was not reduced by anti-DSG3 mAb 5G11 in cells incubated for 24 and 96 h in high-Ca^{2+} medium (n = 4, from 4 independent coating procedures, 2 cell border adhesion maps with 800 force–distance curves/adhesion map, means ± SEM, *$P <$ .05). (**c**) AFM measurements of DSC3-unbinding force in DSG3-KO murine KCs did not show any significant change for both time points (24 and 96 h in high-Ca^{2+} medium) (n = 4, from 4 independent coating procedures, 2 cell border adhesion maps with 800 force–distance curves/adhesion map, means of extreme fits normalized to Ctr ± SEM, *$P <$ .05). (**d**) Schematic of AFM measurement with DSG3-coated tip. The commercial monoclonal anti-DSG2 was binding on the DSG2 ECD2/3 and was solely incubated on the cells to avoid antibody binding to the scanning tip. (**e**) An anti-DSG2 mAb was capable of reducing the binding frequency at both differentiation time points (n = 4, from 4 independent coating procedures, 2 cell border adhesion maps with 800 force–distance curves/adhesion map, means ± SEM, *$P <$ .05). AFM, atomic force microscopy; Ca^{2+}, calcium ion; Ctr, control; DSG, desmoglein; ECD, extracellular domain; KC, keratinocyte; KO, knockout; PEG, polyethylene glycol; WT, wild-type.

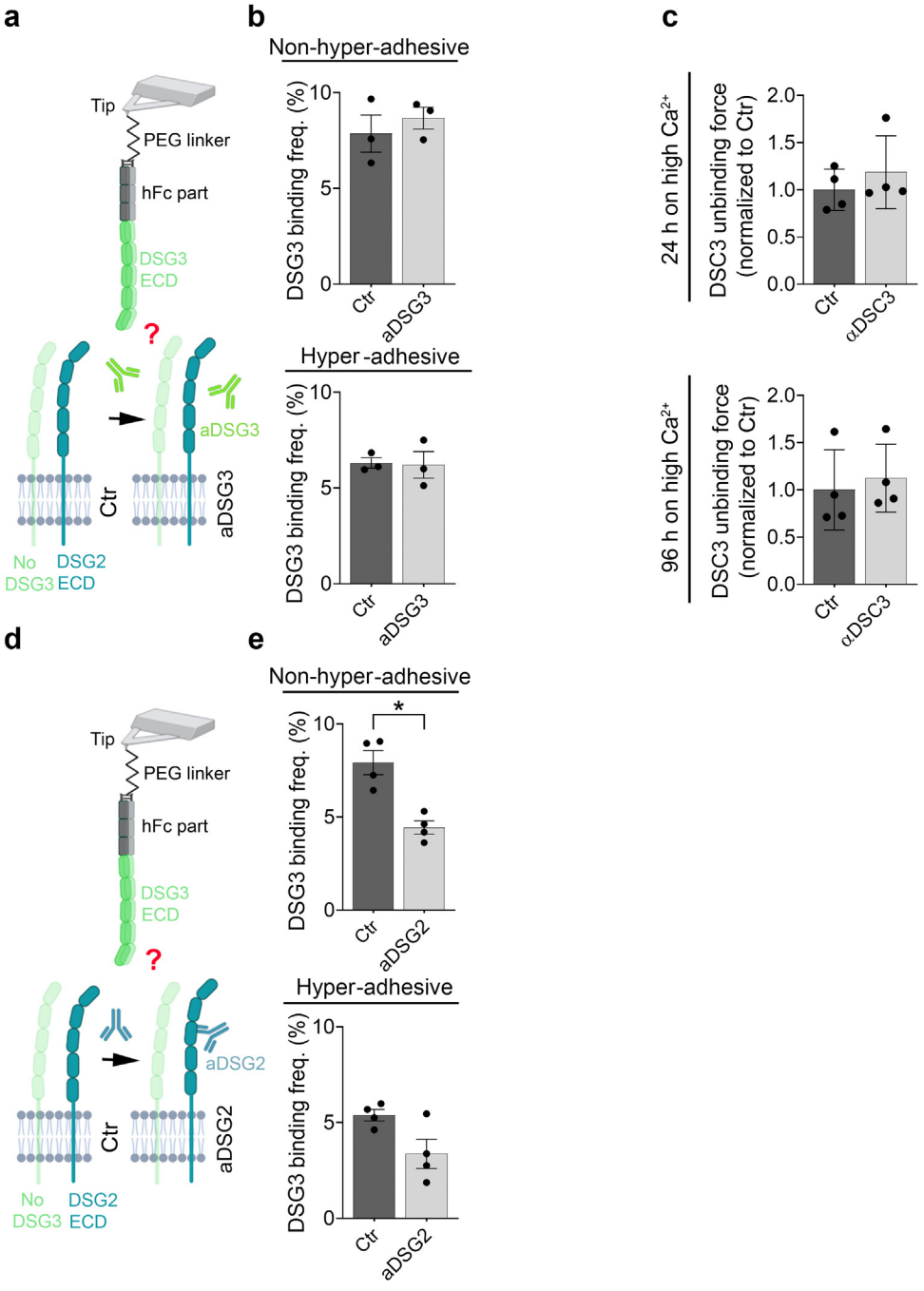

Supplementary Table S1. ELISA Titre and Number of Ethics Vote for Sera from Patients with Pemphigus

Patient Number	ELISA Score (U/ml) Anti-DSG1-IgG	Anti-DSG3-IgG	Ethics Vote Number
PV1	86	171,5	Marburg University Az20/14
PV2	193.2	112.8	Kurume University number 127

Abbreviations: DSG, desmoglein; PV, pemphigus vulgaris.